

# Light-front representation of chiral dynamics with $\Delta$ isobar and large- $N_c$ relations

C. Granados\* and C. Weiss†

*Theory Center, Jefferson Lab, Newport News, VA 23606, USA*

Transverse densities describe the spatial distribution of electromagnetic current in the nucleon at fixed light-front time. At peripheral distances  $b = O(M_\pi^{-1})$  the densities are governed by chiral dynamics and can be calculated model-independently using chiral effective field theory (EFT). Recent work has shown that the EFT results can be represented in first-quantized form, as overlap integrals of chiral light-front wave functions describing the transition of the nucleon to soft-pion-nucleon intermediate states, resulting in a quantum-mechanical picture of the peripheral transverse densities. We now extend this representation to include intermediate states with  $\Delta$  isobars and implement relations based on the large- $N_c$  limit of QCD. We derive the wave function overlap formulas for the  $\Delta$  contributions to the peripheral transverse densities by way of a three-dimensional reduction of relativistic chiral EFT expressions. Our procedure effectively maintains rotational invariance and avoids the ambiguities with higher-spin particles in the light-front time-ordered approach. We study the interplay of  $\pi N$  and  $\pi\Delta$  intermediate states in the quantum-mechanical picture of the densities in a transversely polarized nucleon. We show that the correct  $N_c$ -scaling of the charge and magnetization densities emerges as the result of the particular combination of currents generated by intermediate states with degenerate  $N$  and  $\Delta$ . The off-shell behavior of the chiral EFT is summarized in contact terms and can be studied easily. The methods developed here can be applied to other peripheral densities and to moments of the nucleon's generalized parton distributions.

PACS numbers: 11.10.Ef, 12.39.Fe, 13.40.Gp, 13.60.Hb, 14.20.Dh

Keywords: Elastic form factors, chiral effective field theory, transverse charge and magnetization densities, light-front quantization, Delta isobar

arXiv:1603.08881v1 [hep-ph] 29 Mar 2016

---

\* E-mail: cggranadosj@gmail.com

† E-mail: weiss@jlab.org

## CONTENTS

I. Introduction	3
II. Transverse densities	4
A. Basic properties	4
B. Chiral periphery	6
III. Chiral dynamics with $\Delta$ isobar	7
A. Spinors and propagator	7
B. Coupling to pion	9
IV. Light-front representation with $\Delta$ isobar	10
A. Current matrix element	10
B. Wave function overlap representation	13
C. Polarization states	16
D. Coordinate-space wave function	17
E. Peripheral densities	20
V. Mechanical picture with $\Delta$ isobar	24
A. Transverse polarization	24
B. Mechanical interpretation	26
VI. Large- $N_c$ limit of transverse densities	28
A. Light-front wave functions at large $N_c$	28
B. Contact terms and off-shell behavior	30
VII. Summary and outlook	33
Acknowledgments	34
References	34

## I. INTRODUCTION

Transverse densities are an essential concept in modern studies of hadron structure using theoretical and phenomenological methods [1–4]. They describe the distribution of physical quantities (charge, current, momentum) in the hadron at fixed light-front time  $x^+ \equiv t + z$  and can be computed as the two-dimensional Fourier transforms of the invariant form factors associated with the operators. The transverse densities are frame-independent (invariant under longitudinal boosts) and enable an objective definition of the spatial structure of the hadron as a relativistic system. Their basic properties, connection with the parton picture (generalized parton distributions), and extraction from experimental data, have been discussed extensively in the literature; see Ref. [5] for a review. In particular, the transverse densities offer a new way of identifying the chiral component of nucleon structure and studying its properties [6, 7]. At transverse distances of the order of the inverse pion mass,  $b = O(M_\pi^{-1})$ , the densities are governed by chiral dynamics and can be computed model-independently using methods of effective field theory (EFT). The charge and magnetization densities in the nucleon’s chiral periphery have been studied in a series of articles [7–9]. The densities were computed in the relativistically invariant formulation of chiral EFT, using a dispersive representation that expresses them as integrals over the two-pion cut of the invariant form factors at unphysical momentum transfers  $t > 4M_\pi^2$  [7]. It was further shown that the chiral amplitudes producing the peripheral densities can be represented as physical processes occurring in light-front time, involving the emission and absorption of a soft pion by the nucleon [8, 9]. In this representation the peripheral transverse densities are expressed as overlap integrals of chiral light-front wave functions, describing the transition of the original nucleon to a pion-nucleon state of spatial size  $O(M_\pi^{-1})$  through the chiral EFT interactions. It enables a first-quantized, particle-based view of chiral dynamics, which reveals the role of pion orbital angular momentum and leads to a simple quantum-mechanical picture of peripheral nucleon structure.

Excitation of  $\Delta$  isobars plays an important role in low-energy pion-nucleon dynamics. The  $\Delta$  couples strongly to the  $\pi N$  channel and can contribute to pionic processes, including those producing the peripheral transverse densities. Several extensions of chiral EFT with explicit isobars have been proposed, using different formulations for the spin-3/2 particle [10–12]. Inclusion of the isobar is especially important in view of the large- $N_c$  limit of QCD, which implies general scaling relations for nucleon observables [13–16]. In the large- $N_c$  limit the  $N$  and  $\Delta$  become degenerate,  $M_\Delta - M_N = O(N_c^{-1})$ , and the  $\pi NN$  and the  $\pi N\Delta$  couplings are simply related, so that they have to be included on the same footing. Combination of intermediate  $N$  and  $\Delta$  contributions is generally needed for the chiral EFT results to satisfy the general  $N_c$ -scaling relations [17, 18]; see also Refs. [19, 20]. The effect of the  $\Delta$  on the peripheral transverse densities was studied in the dispersive representation in Ref. [7]. It was observed that the densities obey the correct large- $N_c$  relations if  $N$  and  $\Delta$  contributions are combined; however, no mechanical explanation could be provided in this representation.

In this article we develop the light-front representation of chiral dynamics with  $\Delta$  isobars and implement the large- $N_c$  relations in this framework. We introduce the light-front wave function of the  $N \rightarrow \pi\Delta$  transition in chiral EFT in analogy to the  $N \rightarrow \pi N$  one and derive the overlap representation of the peripheral transverse densities including both  $\pi N$  and  $\pi\Delta$  intermediate states. We then study the effects of the  $\Delta$  in the resulting quantum-mechanical picture and explore the origin of the  $N_c$ -scaling of the transverse densities. The light-front representation with the isobar is of interest for several reasons. First, in the quantum-mechanical picture of the peripheral densities, the  $\pi\Delta$  intermediate states allow for charge and rotational states of the peripheral pion different from those in  $\pi N$  intermediate states, resulting in a rich structure. Second, the  $N_c$ -scaling of the peripheral densities can now be explained in simple mechanical terms, as the result of the cancellation (in the charge density) or addition (in the magnetization density) of the pionic convection current in the  $\pi N$  and  $\pi\Delta$  intermediate states. Third, the light-front representation can be extended to study the  $\Delta$  effects on the nucleon’s peripheral partonic structure (generalized parton distributions), including spin structure [19, 20].

We derive the light-front representation of chiral dynamics with  $\Delta$  isobars by re-writing the relativistically invariant chiral EFT expressions for the current matrix element in a form that corresponds to light-front wave function overlap (three-dimensional reduction), generalizing the method developed for chiral EFT with the nucleon in Ref. [8]. This approach offers several important advantages compared to light-front time-ordered perturbation theory. First, it guarantees exact equivalence of the light-front expressions with the relativistically invariant results. Second, it maintains rotational invariance, which is especially important in calculations with higher-spin particles such as the  $\Delta$ , where breaking of rotational invariance would result in power-like divergences of the EFT loop integrals. Third, it automatically generates the instantaneous (contact) terms in the light-front formulation, which would otherwise have to be determined by extensive additional considerations. The method of Ref. [8] is thus uniquely suited to handle the isobar in light-front chiral EFT and produces unambiguous results with minimal effort. Similar techniques were used in studies of spatially integrated (non-peripheral) nucleon structure in chiral EFT with nucleons in Refs. [21–23].

The extension of relativistic chiral EFT to spin-3/2 isobars is principally not unique. While the on-shell spinor of the spin-3/2 particle is unambiguously defined, the field theory requires off-shell extension of the projector in the propagator (Green function), which is inherently ambiguous [24, 25]. The reason is that relativistic fields with spin  $>$

1/2 involve unphysical degrees of freedom that have to be eliminated by constraints. In the EFT context this ambiguity is contained in the overall reparametrization invariance, which allows one to redefine the fields, changing the off-shell behavior of the propagator and the vertices in a consistent fashion. Several schemes have been proposed for dealing with this ambiguity [10, 11]. Fortunately, as will be shown below, the ambiguity in the field-theoretical formulation does not affect the light-front wave function overlap representation of the peripheral transverse densities in our approach. The differences caused by different off-shell extensions of the EFT reside entirely in contact (instantaneous) terms in the densities and can easily be quantified. We perform our calculations using the relativistic Rarita-Schwinger formulation for the  $\Delta$  propagator and an empirical  $\pi N\Delta$  coupling, but otherwise no explicit off-shell terms at the Lagrangian level. We justify this choice by showing that the sum of  $N$  and  $\Delta$  contributions obeys the correct  $N_c$ -scaling (in both the wave-function overlap and the contact terms), so that no explicit off-shell terms are required from this perspective. This level of treatment is sufficient for our purposes. Going beyond it would require a dynamical criterion to fix the off-shell ambiguity of the EFT.

In our approach to chiral dynamics we consider nucleon structure at “chiral” distances  $b = O(M_\pi^{-1})$ , where we regard the pion mass as parametrically small compared to the “non-chiral” inverse hadronic size but do not consider the limit  $M_\pi \rightarrow 0$  [7]. When introducing the  $\Delta$  isobar in this scheme we do not assume any parametric relation between the  $N$ - $\Delta$  mass splitting and the pion mass. The large- $N_c$  limit is then implemented by assuming the standard scaling relations  $M_\Delta - M_N = O(N_c^{-1})$  and  $M_\pi = O(N_c^0)$ , which implies that the region of chiral distances remains stable in the large- $N_c$  limit,  $b = O(M_\pi^{-1}) = O(N_c^0)$ , as is physically sensible. From a dynamical standpoint, the introduction of the isobar into the chiral EFT changes only the coupling of the peripheral pions to the nucleon, not their propagation to distances  $b = O(M_\pi^{-1})$ , which defines the basic character of the peripheral densities. An advantage of the spatial identification of the chiral region is precisely that it allows us to introduce the isobar in this natural manner.

The plan of the article is as follows. In Sec. II we review the basic features of the transverse densities and their behavior in the chiral periphery. In Sec. III we summarize the description of the isobar in chiral EFT (spinors, propagator, vertices) as relevant for the present calculation. In Sec. IV we derive the light-front representation of the peripheral transverse densities in chiral EFT. This includes the 3-dimensional reduction of the relativistically invariant chiral EFT expressions, the wave function overlap representation, the light-front spin states of  $N$  and  $\Delta$  baryons, the coordinate-space light-front wave functions, and the properties of the transverse densities with  $N$  and  $\Delta$  intermediate states. In Sec. V we discuss the wave function overlap representation with transversely polarized spin states and the resulting quantum-mechanical picture. In Sec. VI we implement the large- $N_c$  relations between the EFT parameters and study the scaling behavior of the chiral light-front wave functions and peripheral transverse densities; we also evaluate the contact term contributions and discuss the role of the off-shell ambiguity in the light-front representation. A summary and outlook are presented in Sec. VII.

The study reported here draws extensively on our previous work [7, 8]. Because the intermediate  $\Delta$  contributions in the light-front representation need to be discussed together with the intermediate  $N$  ones calculated in Ref. [8], some repetition of arguments and quoting of the nucleon expressions is unavoidable to make the presentation readable. Generally, in each step of the derivations in Secs. IV and V, we summarize the basic ideas as formulated in Refs. [7, 8], give the expressions for the intermediate  $N$ , and present the explicit calculations for the  $\Delta$ .

## II. TRANSVERSE DENSITIES

### A. Basic properties

The matrix element of the electromagnetic current between nucleon states with 4-momenta  $p_{1,2}$  and spin quantum numbers  $\sigma_{1,2}$  is of the general form (we follow the conventions of Ref. [7])

$$\langle N(p_2, \sigma_2) | J^\mu(x) | N(p_1, \sigma_1) \rangle = \bar{u}_2 \left[ \gamma^\mu F_1(t) - \frac{\sigma^{\mu\nu} \Delta_\nu}{2M_N} F_2(t) \right] u_1 e^{i\Delta x}, \quad (2.1)$$

where  $u_1 \equiv u(p_1, \sigma_1)$  *etc.* are the nucleon bispinors, normalized to  $\bar{u}_1 u_1 = \bar{u}_2 u_2 = 2M_N$ ;  $\sigma^{\mu\nu} \equiv \frac{1}{2} [\gamma^\mu, \gamma^\nu]$ , and

$$\Delta \equiv p_2 - p_1 \quad (2.2)$$

is the 4-momentum transfer. The dependence on the space-time point  $x$ , where the current is measured, is dictated by translational invariance. The Dirac and Pauli form factors,  $F_1$  and  $F_2$ , are functions of the Lorentz-invariant momentum transfer

$$t \equiv \Delta^2 = (p_2 - p_1)^2, \quad (2.3)$$

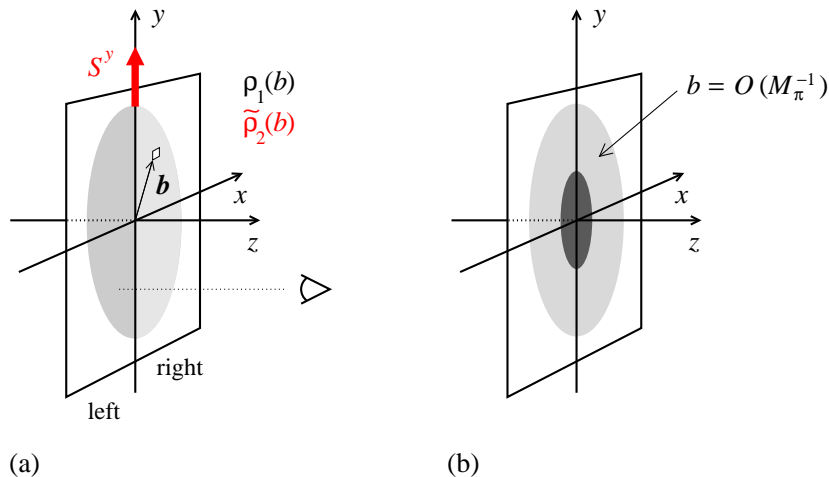


FIG. 1. (a) Interpretation of the transverse densities of the electromagnetic current in a nucleon state with spin quantized in the transverse  $y$ -direction, Eq. (2.6).  $\rho_1(b)$  describes the spin-independent (or left-right symmetric) part of the plus current density;  $\cos\phi\tilde{\rho}_2(b)$  describes the spin-dependent (or left-right asymmetric) part. (b) Peripheral region dominated by chiral dynamics. The central area represents the nucleon's non-chiral hadronic size.

with  $t < 0$  in the physical region for electromagnetic scattering. While the physical content of the invariant form factors can be discussed independently of any reference frame, their space-time interpretation depends on the formulation of relativistic dynamics and on the reference frame.

In the light-front formulation of relativistic dynamics one considers the evolution of strong interactions in light-front time  $x^+ \equiv x^0 + x^3 = x^0 + z$ , as corresponds to clocks synchronized by a light wave traveling through the system in the  $z$ -direction [26–28]. Particle states are characterized by their light-front momentum  $p^+ \equiv p^0 + p^z$  and transverse momentum  $\mathbf{p}_T \equiv (p^x, p^y)$ , while  $p^- \equiv p^0 - p^z = (p_T^2 + M_N^2)/p^+$  plays the role of the energy. In this context it is natural to consider the current matrix element Eq. (2.1) in a class of reference frames where the momentum transfer is in the transverse direction

$$\Delta^\pm = 0, \quad \Delta_T = \mathbf{p}_{2T} - \mathbf{p}_{1T} \neq 0, \quad (2.4)$$

and to represent the form factors as Fourier transforms of certain transverse densities [4, 5]

$$F_{1,2}(t = -\Delta_T^2) = \int d^2b e^{i\Delta_T \cdot \mathbf{b}} \rho_{1,2}(b), \quad (2.5)$$

where  $\mathbf{b} \equiv (b^x, b^y)$  is a 2-dimensional coordinate variable and  $b \equiv |\mathbf{b}|$ . The basic properties of the transverse densities  $\rho_{1,2}(b)$  and their physical interpretation have been discussed in the literature [1–5] and are summarized in Ref. [7]. They describe the transverse spatial distribution of the light-front plus current,  $J^+ \equiv J^0 + J^z$ , in the nucleon at fixed light-front time  $x^+$ . A simple interpretation emerges if the nucleon spin states are chosen as light-front helicity states, which are constructed by preparing rest-frame spin states and boosting them to the desired light-front plus and transverse momentum [7, 28] (see also Sec. IV C below). In a state where the nucleon is localized in transverse space at the origin, and polarized along the  $y$ -direction in the rest frame, the matrix element of the current  $J^+(x)$  at light-front time  $x^+ = 0$  and light-front coordinates  $x^- = 0$  and  $\mathbf{x}_T = \mathbf{b}$  is given by

$$\langle J^+(\mathbf{b}) \rangle_{\text{localized}} = (\dots) [\rho_1(b) + (2S^y) \cos\phi \tilde{\rho}_2(b)], \quad (2.6)$$

$$\tilde{\rho}_2(b) \equiv \frac{\partial}{\partial b} \left[ \frac{\rho_2(b)}{2M_N} \right], \quad (2.7)$$

where (...) stands for a kinematic factor arising from the normalization of the localized nucleon states [7],  $\cos\phi \equiv b^x/b$  is the cosine of the angle of  $\mathbf{b}$  relative to the  $x$ -axis, and  $S^y = \pm 1/2$  is the spin projection on the  $y$ -axis in the nucleon rest frame. One sees that  $\rho_1(b)$  describes the spin-independent part of the current, while the function  $\cos\phi\tilde{\rho}_2(b)$  describes the spin-dependent part of the current in the transversely polarized nucleon (see Fig. 1a).

An alternative interpretation appears if one considers the localized nucleon state with spin  $S^y = +1/2$  and takes the current at two opposite points on the  $x$ -axis,  $\mathbf{b} = \mp b\mathbf{e}_x$ , i.e., on the “left” and “right” when looking at the nucleon from  $z = +\infty$  (see Fig. 1a). According to Eq. (2.6) the current at these points is given by

$$\langle J^+(\mp b\mathbf{e}_x) \rangle_{\text{localized}} = (\dots) [\rho_1(b) \mp \tilde{\rho}_2(b)] \equiv (\dots) \rho_{\text{left/right}}(b), \quad (2.8)$$

such that

$$\left. \begin{array}{l} \rho_1(b) \\ \tilde{\rho}_2(b) \end{array} \right\} = \frac{1}{2} [\pm \rho_{\text{left}}(b) + \rho_{\text{right}}(b)]. \quad (2.9)$$

One sees that  $\rho_1(b)$  and  $\tilde{\rho}_2(b)$  can be interpreted as the left-right symmetric and antisymmetric parts of the plus current on the  $x$ -axis. This representation is useful because the left and right transverse densities have simple properties in dynamical models (positivity, mechanical interpretation). We shall refer to it extensively in the present study [8, 9].

## B. Chiral periphery

At distances  $b = O(M_\pi^{-1})$  the nucleon’s transverse densities are governed by the effective dynamics resulting from the spontaneous breaking of chiral symmetry (see Fig. 1b) [6, 7]. The transverse densities in this region arise from chiral processes in which the current couples to the nucleon through  $t$ -channel exchange of soft pions. In the densities  $\rho_1$  and  $\tilde{\rho}_2$  associated with the electromagnetic current, Eq. (2.1), the leading large-distance component results from the exchange of two pions and occurs in the isovector densities

$$\rho_1^V \equiv \frac{1}{2}(\rho_1^p - \rho_1^n), \quad \tilde{\rho}_2^V \equiv \frac{1}{2}(\tilde{\rho}_2^p - \tilde{\rho}_2^n). \quad (2.10)$$

The large-distance behavior is of the form

$$\left. \begin{array}{l} \rho_1^V(b) \sim P_1(b) \\ \tilde{\rho}_2^V(b) \sim \tilde{P}_2(b) \end{array} \right\} \times \exp(-2M_\pi b). \quad (2.11)$$

The exponential decay is governed by the minimal mass of the exchanged system,  $2M_\pi$ . The pre-exponential factors  $P_1$  and  $\tilde{P}_2$  are determined by the coupling of the exchanged system to the nucleon and exhibit a rich structure, as their dependence on  $b$  is governed by multiple dynamical scales:  $M_\pi$ ,  $M_N$ , and possibly also  $M_\Delta - M_N$ .

In the chiral region  $b = O(M_\pi^{-1})$  the transverse densities can be calculated using chiral EFT [6–9]. The densities can be obtained from the known chiral EFT results for the invariant form factors [29–32]. It is necessary to use chiral EFT with relativistic nucleons [33] in order to reproduce the exact analytic structure of the form factors near the two-pion threshold at  $t = 4M_\pi^2$  (including a sub-threshold singularity on the unphysical sheet), as the latter determines the basic large-distances behavior of the densities, Eq. (2.11). In the LO approximation the processes contributing to the peripheral densities  $\rho_1^V(b)$  and  $\tilde{\rho}_2^V(b)$  are given by the Feynman diagrams of Fig. 2a and b, in which the current couples to the nucleon through two-pion exchange in the  $t$ -channel (explicit expressions will be given below). These processes contribute to the two-pion cut of the form factor and produce densities of the form Eq. (2.11) [6, 7]. Diagrams of Fig. 2c, in which the current couples directly to the nucleon, do not contribute to the two-pion cut of the form factor and produce densities with range  $O(M_N^{-1})$  or terms  $\propto \delta^{(2)}(\mathbf{b})$ . These diagrams renormalize the current at the center of the nucleon and do not need to be considered in the calculation of peripheral densities at  $b = O(M_\pi^{-1})$ .

Excitation of  $\Delta$  isobars contributes to the peripheral transverse densities by modifying the coupling of the two-pion exchange to the nucleon and can be included in the chiral EFT calculations [6, 7]. In a relativistic formulation at LO level the relevant processes are those described by the Feynman diagrams of Fig. 2d and e (explicit expressions will be given below). Diagram Fig. 2d describes the excitation of a dynamical  $\Delta$  through the  $\pi N\Delta$  coupling; diagram Fig. 2e represents possible “new” contact couplings associated with the introduction of the  $\Delta$  into the chiral EFT.

The LO chiral EFT results for the peripheral densities can be represented in two equivalent forms. In the dispersive representation [6, 7] the densities are expressed as integrals over the imaginary parts of the form factor,  $\text{Im } F_{1,2}(t)/\pi$ , on the two-pion cut at  $t > 4M_\pi^2$  (spectral functions). This representation is convenient for studying the asymptotic behavior of the densities, which is related to the behavior of the spectral function near threshold  $t \rightarrow 4M_\pi^2$ . In the light-front representation [8, 9] the densities are expressed as overlap integrals of chiral light-front wave functions, describing the transition of the external nucleon to a pion-nucleon intermediate state of size  $O(M_\pi^{-1})$  through the chiral EFT interactions, as well as contact terms. It enables a first-quantized view of the chiral processes and leads to a simple quantum-mechanical picture of peripheral nucleon structure. Our aim in the following is to derive the light-front representation of the  $\Delta$  contributions.

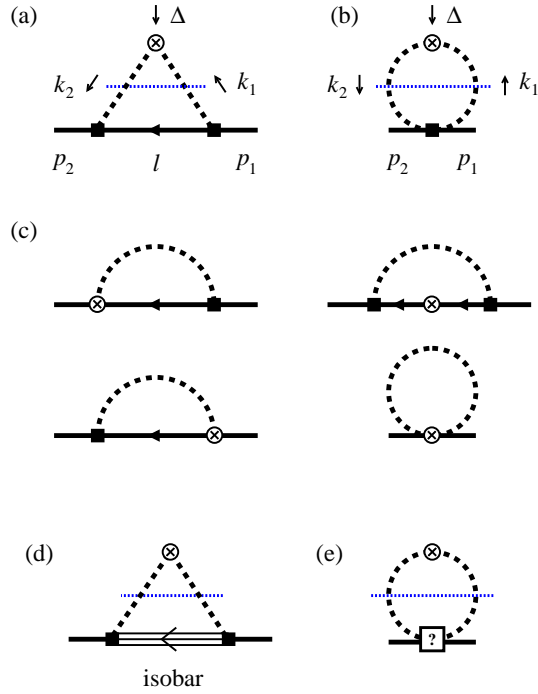


FIG. 2. Feynman diagrams of LO chiral EFT processes contributing to the electromagnetic current matrix element. (a,b)  $\pi N$  diagrams contributing to the two-pion cut (indicated by the dashed blue line), or the peripheral transverse densities. (c) Diagrams not contributing to the two-pion cut, or the peripheral transverse densities. (d, e)  $\pi\Delta$  diagrams contributing to the two-pion cut. Diagram (e) would result from a “new”  $\pi\pi NN$  contact coupling accompanying the introduction of the  $\Delta$  (see Sec. III B).

### III. CHIRAL DYNAMICS WITH $\Delta$ ISOBAR

#### A. Spinors and propagator

We first want to summarize the elements of the field-theoretical description of the  $\Delta$  and its coupling to pions, as needed for the derivation of the light-front representation. The nucleon in relativistically invariant chiral EFT is described by a relativistic spin-1/2 field (Dirac field). The free nucleon state with 4-momentum  $l$ , subject to the mass-shell condition  $l^2 = M_N^2$ , is described by a bispinor  $u(l, \sigma)$  with spin quantum number  $\sigma = \pm 1/2$ , satisfying the Dirac equation ( $\hat{l} \equiv l^\mu \gamma_\mu$ )

$$(\hat{l} - M_N)u(l, \sigma) = 0, \quad (3.1)$$

and normalized such that

$$\bar{u}(l, \sigma_2)u(l, \sigma_1) = 2M_N \delta(\sigma_2, \sigma_1). \quad (3.2)$$

The specific choice of spin polarization in our calculations will be described below (see Sec. IV C). The propagator of the spin-1/2 field with causal boundary condition (Feynman propagator) is

$$G(l) \equiv \frac{\hat{l} + M_N}{l^2 - M_N^2 + i0}, \quad (3.3)$$

where the 4-momentum is generally off mass-shell,  $l^2 \neq M_N^2$ , and the residue at the pole at  $l^2 = M_N^2$  is the projector on nucleon states,

$$(\hat{l} + M_N)|_{l^2=M_N^2} = \sum_{\sigma} u(l, \sigma)\bar{u}(l, \sigma). \quad (3.4)$$

The isobar in relativistic EFT is described by a relativistic spin-3/2 field. The general procedure is to construct this field as the product of a spin-1 (vector) and a spin-1/2 (spinor) field and eliminate the spin-1/2 degrees of freedom

through constraints formulated in a relativistically covariant manner (Rarita-Schwinger formulation); see Ref. [10] for a review. The free isobar state with 4-momentum  $l$ , subject to the mass-shell condition  $l^2 = M_\Delta^2$ , is described by a vector-bispinor

$$U^\mu(l, \sigma) \equiv \sum_{\lambda\sigma'} C_{1,\lambda; 1/2,\sigma'}^{3/2,\sigma} \epsilon^\mu(l, \lambda) u(l, \sigma'), \quad (3.5)$$

with spin quantum number  $\sigma = (-3/2, -1/2, 1/2, 3/2)$ . Here

$$C_{1,\lambda; 1/2,\sigma'}^{3/2,\sigma} \equiv \langle 1\lambda, \frac{1}{2}\sigma' | \frac{3}{2}, \sigma \rangle \quad (3.6)$$

is the vector coupling coefficient for angular momenta  $1 + \frac{1}{2} \rightarrow \frac{3}{2}$ ;  $\epsilon^\mu(l, \lambda)$  is the polarization vector of a spin-1 particle with 4-momentum  $l$  and spin quantum number  $\lambda = (-1, 0, 1)$  and satisfies

$$l^\mu \epsilon_\mu(l, \lambda) = 0, \quad (3.7)$$

$$\sum_\lambda \epsilon^\mu(l, \lambda) \epsilon^\nu(l, \lambda) = -g^{\mu\nu} + \frac{l^\mu l^\nu}{M_\Delta^2}; \quad (3.8)$$

and  $u(l, \sigma')$  is a bispinor with spin quantum number  $\sigma' = \pm 1/2$  and mass  $M_\Delta$  and satisfies [cf. Eqs. (3.1) and (3.2)]

$$(\hat{l} - M_\Delta)u(l, \sigma') = 0, \quad (3.9)$$

$$\bar{u}(l, \sigma'')u(l, \sigma') = 2M_\Delta \delta(\sigma'', \sigma'), \quad (3.10)$$

$$(\hat{l} + M_\Delta)|_{l^2=M_\Delta^2} = \sum_{\sigma'} u(l, \sigma') \bar{u}(l, \sigma'). \quad (3.11)$$

As a result the vector-bispinor Eq. (3.5) satisfies the conditions

$$(\hat{l} - M_\Delta)U^\mu = 0, \quad (3.12)$$

$$l^\mu U_\mu = 0. \quad (3.13)$$

The constraint Eq. (3.7) eliminates spin-0 states and ensures that the polarization vector describes only spin-1 states in the rest frame. Equation (3.13) therefore implies that the vector-bispinor contains only spin-3/2 degrees of freedom in the rest frame. The normalization of the vector-bispinor is such that

$$\bar{U}^\mu(l, \sigma_2)U_\mu(l, \sigma_1) = -2M_\Delta \delta(\sigma_2, \sigma_1). \quad (3.14)$$

The propagator of the relativistic spin-3/2 field is of the general form

$$G^{\mu\nu}(l) \equiv \frac{R^{\mu\nu}(l)}{l^2 - M_\Delta^2 + i0}, \quad (3.15)$$

where  $R^{\mu\nu}(l)$  represents a 4-tensor and matrix in bispinor indices and is defined for arbitrary 4-momenta  $l$ , not necessarily restricted to the mass shell. On the mass shell  $l^2 = M_\Delta^2$ , i.e., at the pole of the propagator,  $R^{\mu\nu}(l)$  coincides with the projector on isobar states [cf. Eq. (3.4)]

$$R^{\mu\nu}(l)|_{l^2=M_\Delta^2} = \sum_\sigma U^\mu(l, \sigma) \bar{U}^\nu(l, \sigma). \quad (3.16)$$

On the mass shell it therefore satisfies the constraints [cf. Eqs. (3.12) and (3.13)]

$$\left. \begin{array}{l} l_\mu R^{\mu\nu} \\ R^{\mu\nu} l_\nu \\ (\hat{l} - M_\Delta)R^{\mu\nu} \\ R^{\mu\nu}(\hat{l} - M_\Delta) \end{array} \right\} = 0 \quad \text{at} \quad l^2 = M_\Delta^2. \quad (3.17)$$

An explicit representation of  $R^{\mu\nu}(l)$  on the mass shell is

$$R^{\mu\nu}(l)|_{l^2=M_\Delta^2} = (\hat{l} + M_\Delta) \left[ -g^{\mu\nu} + \frac{1}{3}\gamma^\mu \gamma^\nu + \frac{2}{3M_\Delta^2} l^\mu l^\nu - \frac{1}{3M_\Delta} (l^\mu \gamma^\nu - \gamma^\mu l^\nu) \right] \quad (3.18)$$

$$= (\hat{l} + M_\Delta) \left( -g^{\mu\nu} + \frac{l^\mu l^\nu}{M_\Delta^2} \right) - \frac{1}{3} \left( \gamma^\mu + \frac{l^\mu}{M_\Delta} \right) (\hat{l} - M_\Delta) \left( \gamma^\nu + \frac{l^\nu}{M_\Delta} \right). \quad (3.19)$$

The extension of the function  $R^{\mu\nu}(l)$  to off mass-shell momenta  $l^2 \neq M_\Delta^2$  is inherently not unique [24, 25]. The reason is that the physical constraints eliminating the spin-1/2 content of the field can be formulated unambiguously only for on-shell momenta. Any tensor-bispinor matrix function  $R^{\mu\nu}(l)$  that satisfies the conditions Eq. (3.17) on-shell represents a valid propagator Eq. (3.15). In EFT this ambiguity in the definition of the propagator is accompanied by a similar ambiguity in the definition of the vertices and contained in the overall reparametrization invariance of the theory, i.e., the freedom of redefining the fields off mass-shell [10]. For our purposes — deriving the light-front wave function representation of the isobar contributions to the transverse densities — this ambiguity will be largely unimportant, as it shows up only in contact terms where its effects can easily be quantified. We can therefore perform our calculation with a specific choice of the spin-3/2 propagator. *We define* the spin-3/2 propagator by using in Eq. (3.15) the expression for  $R^{\mu\nu}(l)$  given by the off-shell extension of the expressions in Eq. (3.18) or (3.19) (note that the two expressions are algebraically equivalent also for off-shell momenta). This choice represents the natural generalization of the projector to off-shell momenta and leads to simple expressions for the isobar contributions to the transverse densities and other nucleon observables. We shall justify this choice a posteriori by showing that the resulting isobar contributions obey the correct large- $N_c$  relations when combined with the nucleon contributions (see Sec. VI B).

## B. Coupling to pion

The interaction of the nucleon with pions are constrained by chiral invariance. The explicit vertices emerge from the expansion of the non-linear chiral Lagrangian in pion field [33]. The vertices governing the LO chiral processes in the diagrams of Fig. 2a and b are contained in

$$\mathcal{L}_{\pi NN} = -\frac{g_A}{2F_\pi} \bar{\psi}_j \gamma^\mu \gamma_5 (\tau^a)_i^j \psi^i \partial_\mu \pi^a - \frac{1}{4F_\pi^2} \bar{\psi}_j \gamma^\mu (\tau^a)_i^j \psi^i \epsilon^{abc} \pi^b \partial_\mu \pi^c, \quad (3.20)$$

where  $\psi^i = (\psi^p, \psi^n)$  is the isospin-1/2 nucleon field,  $\pi^a = (\pi^1, \pi^2, \pi^3)$  are the real (cartesian) components of the isospin-1 pion field, and summation over isospin indices is implied. The first term in Eq. (3.20) describes a three-point  $\pi NN$  coupling. The axial vector vertex is equivalent to the conventional pseudoscalar vertex under the conditions that (i) the nucleons are on-shell; (ii) 4-momenta at the vertex are conserved, i.e., the pion 4-momentum is equal to the difference of the nucleon 4-momenta, as is the case in Feynman perturbation theory. The relation is:

$$-\frac{g_A}{2F_\pi} \bar{u}(l') i(\hat{l}' - \hat{l}) \gamma_5 \tau^a u(l) = \frac{g_A M_N}{F_\pi} \bar{u}(l') i \gamma_5 \tau^a u(l) \equiv g_{\pi NN} \bar{u}(l') i \gamma_5 \tau^a u(l). \quad (3.21)$$

In terms of the complex (spherical) components of the pion field the first term in Eq. (3.20) reads

$$-\frac{g_A}{2F_\pi} \left( \sqrt{2} \bar{\psi}_n \gamma^\mu \gamma_5 \partial_\mu \pi^+ \psi_p + \sqrt{2} \bar{\psi}_p \gamma^\mu \gamma_5 \partial_\mu \pi^+ \psi_n + \bar{\psi}_p \gamma^\mu \gamma_5 \partial_\mu \pi^0 \psi_p - \bar{\psi}_n \gamma^\mu \gamma_5 \partial_\mu \pi^0 \psi_n \right). \quad (3.22)$$

The second term in Eq. (3.20) represents a four-point  $\pi\pi NN$  coupling. It arises due to chiral invariance, as can be seen in the fact that its coupling is completely given in terms of  $F_\pi$  and does not involve any dynamical parameters. In LO the parameters are taken at their physical values  $g_A = 1.26$  and  $F_\pi = 93$  MeV.

The coupling of the  $\Delta$  isobar to the  $\pi N$  system is likewise constrained by chiral invariance [10]. The unique structure emerging as the first-order expansion in the pion field of the nonlinear chirally invariant  $\pi N \Delta$  Lagrangian is

$$\mathcal{L}_{\pi N \Delta} \sim \frac{i g_{\pi N \Delta}}{M_N} C_{1,k; 1/2,i}^{3/2,j} \bar{\psi}^i \partial_\mu \pi^k \Psi^{\mu j} + \text{h.c.}, \quad (3.23)$$

where  $\Psi_\Delta^{\mu j} = (\Psi_{\Delta^{++}}^\mu, \Psi_{\Delta^+}^\mu, \Psi_{\Delta^0}^\mu, \Psi_{\Delta^-}^\mu)$  is the isobar field,  $\pi^k = (\pi^+, \pi^-, \pi^0)$  are the complex (spherical) components of the pion field, and  $C_{1,k; 1/2,i}^{3/2,j}$  denotes the isospin vector coupling coefficient in the appropriate representation. In terms of the individual isospin components the couplings are

$$\begin{aligned} \mathcal{L}_{\pi N \Delta} = & \frac{i g_{\pi N \Delta}}{\sqrt{2} M_N} \left( \bar{\psi}_p \partial_\mu \pi^- \Psi_{\Delta^{++}}^\mu + \sqrt{\frac{2}{3}} \bar{\psi}_p \partial_\mu \pi^0 \Psi_{\Delta^+}^\mu + \frac{1}{\sqrt{3}} \bar{\psi}_p \partial_\mu \pi^+ \Psi_{\Delta^0}^\mu \right. \\ & \left. + \bar{\psi}_n \partial_\mu \pi^+ \Psi_{\Delta^-}^\mu + \sqrt{\frac{2}{3}} \bar{\psi}_n \partial_\mu \pi^0 \Psi_{\Delta^0}^\mu + \frac{1}{\sqrt{3}} \bar{\psi}_n \partial_\mu \pi^- \Psi_{\Delta^+}^\mu \right) + \text{h.c.} \end{aligned} \quad (3.24)$$

The empirical value of the  $\pi N \Delta$  coupling is  $g_{\pi N \Delta} = 20.22$ .

The introduction of the  $\Delta$  into chiral EFT could in principle be accompanied by “new”  $\pi\pi NN$  contact terms in the Lagrangian, of the form of the second term in Eq. (3.20), or with other structures. Physically such terms describe short-distance degrees of freedom that are integrated out in the derivation of the effective theory. They contain dynamical information and cannot be determined from the symmetries alone. We do not introduce any explicit contact terms at this time; their contributions can easily be included later. We shall justify this choice a posteriori, by showing that the large- $N_c$  relations between the densities resulting from  $N$  and  $\Delta$  intermediate states are satisfied without explicit contact terms. We note that this ambiguity is related to that resulting from the off-shell extension of the propagator (see Sec. III A). It will be seen that both result in identical contact term contributions to the transverse densities in the light-front representation.

#### IV. LIGHT-FRONT REPRESENTATION WITH $\Delta$ ISOBAR

##### A. Current matrix element

We now derive the light-front representation of the peripheral transverse densities including the  $\Delta$  isobar contribution, following the approach developed in Ref. [8] for chiral EFT with nucleons only. The first step is to compute the peripheral contributions to the current matrix element Eq. (2.1) from the processes Fig. 2a and b (nucleon) and Fig. 2d (isobar) in terms of Feynman integrals, and to separate each one of them into two parts:

- (i) An “intermediate-baryon” term, which contains the intermediate-baryon pole of the triangle diagram at  $l^2 = M_B^2$  ( $B = N, \Delta$ ). This term will then be evaluated as a contour integral over the light-front energy variable and represented as an overlap integral of  $N \rightarrow \pi B$  light-front wave functions.
- (ii) A “contact” term, which combines (a) contributions from the triangle graph in which the intermediate-baryon pole is canceled by factors  $l^2 - M_B^2$  arising from the numerator of the Feynman integral; (b) contributions from the diagram involving the explicit  $\pi\pi NN$  vertices in the Lagrangian.

The separation becomes unique if we require that the numerator of intermediate-baryon term do not contain finite powers in  $l^2 - M_B^2$ , i.e., that they are all absorbed in the contact term. In performing the separation we use the specific off-shell behavior of the EFT propagators and vertices. We also systematically neglect non-peripheral contributions to the current matrix element, i.e., terms that do not contribute to the two-pion cut.

The nucleon EFT contribution to the peripheral isovector current matrix element results from the two diagrams of Fig. 2a and b and is given by

$$\begin{aligned} \langle N_2 | J^\mu(0) | N_1 \rangle_N^V &\equiv \langle N(p_2, \sigma_2) | J^\mu(0) | N(p_1, \sigma_1) \rangle_N^V \\ &= \frac{g_A^2}{2F_\pi^2} \int \frac{d^4k}{(2\pi)^4} \frac{(-i)(2k^\mu) \bar{u}_2 i \hat{k}_2 \gamma_5 (\hat{l} + M_N) i \hat{k}_1 \gamma_5 u_1}{(k_1^2 - M_\pi^2 + i0)(k_2^2 - M_\pi^2 + i0)(l^2 - M_N^2 + i0)} \\ &+ \frac{1}{2F_\pi^2} \int \frac{d^4k}{(2\pi)^4} \frac{i(2k^\mu) \bar{u}_2 \hat{k} u_1}{(k_1^2 - M_\pi^2 + i0)(k_2^2 - M_\pi^2 + i0)}, \end{aligned} \quad (4.1)$$

where  $k_{1,2} = k \mp \Delta, l = p_1 - k_1 = p_2 - k_2$ , and the integration is over the average pion 4-momentum  $k$ . In the numerators the vector  $2k^\mu$  represents the vector current of the charged pion. Using the anticommutation relations between the gamma matrices and the Dirac equation for the nucleon spinors the numerator of the triangle diagram, Eq. (4.1), can be rewritten as

$$\frac{g_A^2}{2F_\pi^2} \bar{u}_2 i \hat{k}_2 \gamma_5 (\hat{l} + M_N) i \hat{k}_1 \gamma_5 u_1 = \frac{2g_A^2 M_N^2}{F_\pi^2} \bar{u}_2 \hat{k} u_1 + \frac{g_A^2}{2F_\pi^2} (l^2 - M_N^2) [\bar{u}_2 \hat{k} u_1 + \dots] \quad (4.3)$$

In the second term the factor  $(l^2 - M_N^2)$  cancels the nucleon pole in Eq. (4.1). This term thus results in an integral of the same form as the contact diagram, Eq. (4.2). The (...) in Eq. (4.3) stands for terms that are even under  $k \rightarrow -k$  and drop out in the integral, as the remaining integrand is odd under  $k \rightarrow -k$ , cf. Eq. (4.2). The total nucleon contribution can thus be represented as

$$\langle N_2 | J^\mu(0) | N_1 \rangle_N^V = \int \frac{d^4k}{(2\pi)^4} \frac{i(2k^\mu) A_{N, \text{interm}}}{(k_1^2 - M_\pi^2 + i0)(k_2^2 - M_\pi^2 + i0)(l^2 - M_N^2 + i0)} \quad (4.4)$$

$$+ \int \frac{d^4k}{(2\pi)^4} \frac{i(2k^\mu) A_{N, \text{cont}}}{(k_1^2 - M_\pi^2 + i0)(k_2^2 - M_\pi^2 + i0)}, \quad (4.5)$$

$$A_{N, \text{interm}} = -\frac{2g_A^2 M_N^2}{F_\pi^2} \bar{u}_2 \hat{k} u_1, \quad (4.6)$$

$$A_{N, \text{cont}} = \frac{1 - g_A^2}{2F_\pi^2} \bar{u}_2 \hat{k} u_1. \quad (4.7)$$

By construction, for 4-momenta on the nucleon mass shell,  $l^2 = M_N^2$ , the numerator Eq. (4.6) coincides with the numerator of the original triangle diagram, Eq. (4.1),

$$A_{N, \text{interm}}|_{l^2=M_N^2} = -\frac{g_A^2}{2F_\pi^2} [\bar{u}_2 i \hat{k}_2 \gamma_5 (\hat{l} + M_N) i \hat{k}_1 \gamma_5 u_1]_{l^2=M_N^2}. \quad (4.8)$$

The isobar contribution to the peripheral current matrix element resulting from diagram Fig. 2d is given by

$$\langle N_2 | J^\mu(0) | N_1 \rangle_\Delta^V = \frac{g_{\pi N \Delta}^2}{3M_N^2} \int \frac{d^4 k}{(2\pi)^4} \frac{(-i)(2k^\mu) [\bar{u}_2 k_{2\alpha} R^{\alpha\beta}(l) k_{1\beta} u_1]}{(k_2^2 - M_\pi^2 + i0)(k_1^2 - M_\pi^2 + i0)(l^2 - M_\Delta^2 + i0)}. \quad (4.9)$$

The bilinear form in the numerator is an invariant function of the 4-vectors  $p_1, p_2$  and  $k$  (for given spin quantum numbers of the external nucleon spinors,  $\sigma_1$  and  $\sigma_2$ ). Using the specific form of  $R^{\alpha\beta}(l)$ , as given by Eqs. (3.18) and (3.19) without the mass-shell condition, and employing gamma matrix identities and the Dirac equation for the external nucleon spinors, the bilinear form can be represented as

$$\bar{u}_2 k_{2\alpha} R^{\alpha\beta}(l) k_{1\beta} u_1 = \bar{u}_2 (\mathcal{F} + \mathcal{G} \hat{k}) u_1. \quad (4.10)$$

Here  $\mathcal{F}$  and  $\mathcal{G}$  are scalar functions of four independent invariants formed from the 4-vectors  $p_1, p_2$  and  $k$ . We choose as independent invariants  $k_1^2, k_2^2, l^2$  and  $t$ , and write

$$\mathcal{F}, \mathcal{G} = \text{functions}(k_1^2, k_2^2, l^2, t). \quad (4.11)$$

Because the functions arise from the contraction of finite-rank tensors, their dependence on the invariants is polynomial, and we can expand them around the position of the poles of the propagators in Eq. (4.9). In the expansion in  $k_1^2 - M_\pi^2$  and  $k_2^2 - M_\pi^2$  we keep only the zeroth order term, as any finite power of  $k_{1,2}^2 - M_\pi^2$  would cancel the pole of one of the pion propagators and thus no longer contribute to the two-pion cut (such contributions would be topologically equivalent to those of the diagrams of Fig. 2c, which we also neglect). In the expansion in  $l^2 - M_\Delta^2$  we keep all terms, and write the result as the sum of the zeroth order term and a remainder summing up the powers  $(l^2 - M_\Delta^2)^k$  with  $k \geq 1$ . In this way the bilinear form becomes

$$\begin{aligned} \bar{u}_2 k_{2\alpha} R^{\alpha\beta}(l) k_{1\beta} u_1 &= \bar{u}_2 (F + G \hat{k}) u_1 + (l^2 - M_\Delta^2) \bar{u}_2 (F_{\text{cont}} + G_{\text{cont}} \hat{k}) u_1 \\ &+ \text{terms} \sim (k_{1,2}^2 - M_\pi^2), \end{aligned} \quad (4.12)$$

where

$$F \equiv \mathcal{F}(k_1^2 = M_\pi^2, k_2^2 = M_\pi^2, l^2 = M_\Delta^2, t), \quad (4.13)$$

$$F_{\text{cont}} \equiv \frac{\mathcal{F}(k_1^2 = M_\pi^2, k_2^2 = M_\pi^2, l^2, t) - \mathcal{F}(\dots, l^2 = M_\Delta^2, \dots)}{l^2 - M_\Delta^2}, \quad (4.14)$$

and similarly for  $G$  and  $G_{\text{cont}}$  in terms of  $\mathcal{G}$ . The explicit expressions are

$$\begin{aligned} F &\equiv \left[ \frac{t}{2} - M_N^2 + \frac{(M_\Delta^2 + M_N^2 - M_\pi^2)^2}{4M_\Delta^2} \right] (M_N + M_\Delta) \\ &- \frac{1}{3} \left( M_N + \frac{M_\Delta^2 + M_N^2 - M_\pi^2}{2M_\Delta} \right)^2 (M_N - M_\Delta), \end{aligned} \quad (4.15)$$

$$\begin{aligned} G &\equiv - \left[ \frac{t}{2} - M_N^2 + \frac{(M_\Delta^2 + M_N^2 - M_\pi^2)^2}{4M_\Delta^2} \right] \\ &+ \frac{1}{3} \left( M_N + \frac{M_\Delta^2 + M_N^2 - M_\pi^2}{2M_\Delta} \right)^2, \end{aligned} \quad (4.16)$$

$$F_{\text{cont}} \equiv \frac{1}{3M_{\Delta}^2}(M_{\Delta}^2 - M_N^2 + M_N M_{\Delta} + M_{\pi}^2)(M_N + M_{\Delta}) + \frac{(l^2 - M_{\Delta}^2)}{6M_{\Delta}^2}M_N, \quad (4.17)$$

$$G_{\text{cont}} \equiv -\frac{1}{3M_{\Delta}^2}(M_{\Delta}^2 - M_N^2 + M_N M_{\Delta} + M_{\pi}^2) - \frac{(l^2 - M_{\Delta}^2)}{6M_{\Delta}^2}. \quad (4.18)$$

The isobar contribution can thus be represented as

$$\langle N_2 | J^{\mu}(0) | N_1 \rangle_{\Delta}^V = \int \frac{d^4 k}{(2\pi)^4} \frac{i(2k^{\mu}) A_{\Delta, \text{interm}}}{(k_1^2 - M_{\pi}^2 + i0)(k_2^2 - M_{\pi}^2 + i0)(l^2 - M_N^2 + i0)} \quad (4.19)$$

$$+ \int \frac{d^4 k}{(2\pi)^4} \frac{i(2k^{\mu}) A_{\Delta, \text{cont}}}{(k_1^2 - M_{\pi}^2 + i0)(k_2^2 - M_{\pi}^2 + i0)}, \quad (4.20)$$

$$A_{\Delta, \text{interm}} = -\frac{g_{\pi N \Delta}^2}{3M_N^2} \bar{u}_2(F + G \hat{k})u_1, \quad (4.21)$$

$$A_{\Delta, \text{cont}} = -\frac{g_{\pi N \Delta}^2}{3M_N^2} \bar{u}_2(F_{\text{cont}} + G_{\text{cont}} \hat{k})u_1, \quad (4.22)$$

which is analogous to Eqs. (4.4)-(4.7) for the nucleon. By construction, for 4-momenta on the  $\Delta$  mass shell,  $l^2 = M_{\Delta}^2$ , the numerator Eq. (4.21) coincides with the numerator of the original triangle diagram, Eq. (4.9),

$$A_{\Delta, \text{interm}}|_{l^2=M_{\Delta}^2} = -\frac{g_{\pi N \Delta}^2}{3M_N^2} [\bar{u}_2 k_{2\alpha} R^{\alpha\beta}(l) k_{1\beta} u_1]_{l^2=M_N^2}. \quad (4.23)$$

Combining nucleon and isobar contributions, the total peripheral current in chiral EFT can be represented as

$$\langle N_2 | J^{\mu}(0) | N_1 \rangle^V = \sum_{B=N, \Delta} \langle N_2 | J^{\mu}(0) | N_1 \rangle_B^V \quad (4.24)$$

$$\langle N_2 | J^{\mu}(0) | N_1 \rangle_B^V = \int \frac{d^4 k}{(2\pi)^4} \frac{i(2k^{\mu}) A_{B, \text{interm}}}{(k_1^2 - M_{\pi}^2 + i0)(k_2^2 - M_{\pi}^2 + i0)(l^2 - M_B^2 + i0)} \quad (4.25)$$

$$+ \int \frac{d^4 k}{(2\pi)^4} \frac{i(2k^{\mu}) A_{B, \text{cont}}}{(k_1^2 - M_{\pi}^2 + i0)(k_2^2 - M_{\pi}^2 + i0)}, \quad (4.26)$$

with numerators given by the specific expressions Eqs. (4.6), (4.7), (4.21) and (4.22). These expressions will be used subsequently to derive the light-front wave function overlap representation of the current matrix element.

The intermediate-baryon term of the peripheral current is independent of the off-shell behavior of the propagator and vertices, both in the  $N$  and  $\Delta$  case. Because the numerator is evaluated at  $k_{1,2}^2 = M_{\pi}^2$  (two-pion cut, or peripheral distances) and  $l^2 = M_B^2$  (definition of intermediate-baryon term), the intermediate-baryon term effectively corresponds to the ‘‘triple cut’’ triangle diagram in which all internal lines are on mass-shell.<sup>1</sup> It thus expresses the physical particle content of the effective theory. The off-shell behavior enters only in the effective contact terms. In particular, the addition of an explicit new  $\pi\pi NN$  contact term in connection with the  $\Delta$  [cf. diagram Fig. 2e] would modify only the effective contact term in Eq. (4.26).

Some comments are in order regarding the ultraviolet (UV) behavior of the Feynman integrals. As they stand, the Feynman integrals Eqs. (4.4)-(4.7) and Eqs. (4.19)-(4.22) are UV divergent. In the dispersive approach the peripheral

---

<sup>1</sup> Such ‘‘completely cut’’ diagrams describe absorptive parts in unphysical regions of the external kinematic variables and are used in the dispersive representation of multiparticle amplitudes (Mandelstam representation) [34].

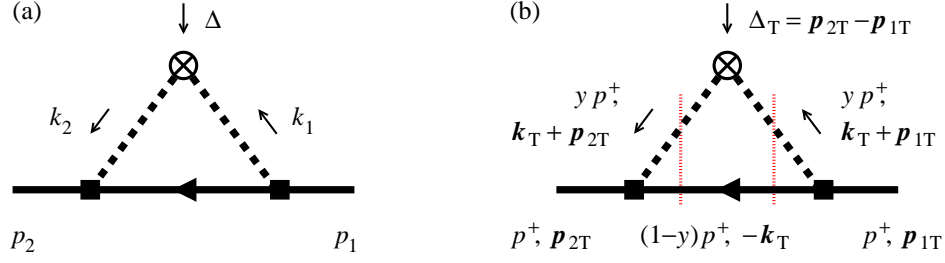


FIG. 3. Wave function overlap representation of the intermediate-baryon Feynman integral. (a) Feynman integral Eq. (4.25) with 4-momenta. (b) Light-front components of momenta in frame where  $\Delta$  is transverse, Eq. (4.27).

densities are computed using only the imaginary part of the form factors on the two-pion cut, which is UV finite. In the present calculation the Feynman integrals could be regularized in a Lorentz-invariant manner, e.g. by subtraction of the integrals at  $t = 0$ ; such subtractions would correspond to a modification of the transverse density by delta functions at  $b = 0$  and do not affect the peripheral densities. In the wave function overlap representation derived in the following section, the regularization happens “automatically” when we change to the coordinate representation and compute the densities at non-zero transverse distance. We thus do not need to explicitly regularize the integrals at this stage.

### B. Wave function overlap representation

The next step is to represent the intermediate-baryon term of the current matrix element, Eq. (4.25), as an overlap integral of light-front wave functions describing the  $N \rightarrow \pi B$  transition ( $B = N, \Delta$ ) [8]. This is accomplished by performing a three-dimensional reduction of the Feynman integral using light-front momentum variables. The integral over the light-front energy is performed by contour integration, closing the contour around the baryon pole, where the baryon momentum is on mass-shell and the numerator can be replaced by the on-shell projector.

The reduction is performed in a frame where the momentum transfer has only transverse components, cf. Eq. (2.4), such that (see Fig. 3)

$$p_1^+ = p_2^+ \equiv p^+, \quad \mathbf{p}_{2T} - \mathbf{p}_{1T} = \Delta_T, \quad p_1^- = \frac{M_N^2 + \mathbf{p}_{1T}^2}{p^+}, \quad p_2^- = \frac{M_N^2 + \mathbf{p}_{2T}^2}{p^+}. \quad (4.27)$$

Here  $p^+ > 0$  is a free parameter which selects a particular frame in a class of frames related by longitudinal boosts. The transverse momenta satisfy  $\mathbf{p}_{2T} - \mathbf{p}_{1T} = \Delta_T$ , while the overall transverse momentum remains unspecified. The loop momentum is described by its light-front components  $k^\pm \equiv k^0 \pm k^z$  and  $\mathbf{k}_T \equiv (k^x, k^y)$ , and  $k^+$  is parametrized in terms of the boost-invariant light-front momentum fraction of the pion,

$$y \equiv k^+/p^+. \quad (4.28)$$

The integrand of the Feynman integral Eq. (4.25) has simple poles in  $k^-$  and can be computed by closing the contour around the pole of the baryon propagator [8]. Here it is essential that we have organized the contributions in Eqs. (4.25) and (4.26) such that the integrand of Eqs. (4.25) does not contain any non-zero powers of  $l^2 - M_B^2$ , which would be “invisible” at the baryon pole; [they are contained in the contact term Eq. (4.26)]. At the baryon pole in  $k^-$  the pion virtualities are, up to a factor, given by the invariant mass differences between the external nucleon and the pion-baryon system in the intermediate state (here  $\bar{y} \equiv 1 - y$ ),

$$-\frac{k_1^2 - M_\pi^2}{y} = \frac{(\mathbf{k}_T + \bar{y}\mathbf{p}_{1T})^2 + M_\pi^2}{y} + \frac{(\mathbf{k}_T + \bar{y}\mathbf{p}_{1T})^2 + M_B^2}{\bar{y}} - M_N^2. \equiv \Delta \mathcal{M}_{N \rightarrow \pi B}^2(y, \mathbf{k}_T, \mathbf{p}_{1T}), \quad (4.29)$$

and similarly for  $k_1 \rightarrow k_2$  and  $\mathbf{p}_{1T} \rightarrow \mathbf{p}_{2T}$ . This allows us to convert the pion denominators in the Feynman integral into light-front energy denominators for the  $N \rightarrow \pi B$  transition and back.

Furthermore, at the baryon pole in  $k^-$  the numerator of the Feynman integral can be factorized. At the pole the baryon 4-momentum is on mass shell,  $l^2 = M_N^2$ . By construction the numerator of the intermediate-baryon Feynman integral Eq. (4.25) is equal to the numerator of the original Feynman integral on the baryon mass shell. At the same time, on the mass shell the residue of the baryon propagator in the original Feynman integral can be replaced

by the projector on on-shell baryon spinors (or vector-spinors) with 4-momentum  $l$ . For the intermediate nucleon contribution, using Eqs. (4.8) and (3.4), we get [here  $u_1 \equiv u(p_1, \sigma_1)$ ,  $u_2 \equiv u(p_2, \sigma_2)$  and  $u \equiv u(l, \sigma)$ ]

$$A_{N, \text{interm}} = -\frac{g_A^2}{2F_\pi^2} [\bar{u}_2 i \hat{k}_2 \gamma_5 (\hat{l} + M_N) i \hat{k}_1 \gamma_5 u_1]_{l^2=M_N^2} \quad (4.30)$$

$$= -\frac{g_A^2}{2F_\pi^2} \sum_\sigma [\bar{u}_2 i \hat{k}_2 \gamma_5 u] [\bar{u} i \hat{k}_1 \gamma_5 u_1] \quad (\sigma = \pm \frac{1}{2}) \quad (4.31)$$

$$= 2 \sum_\sigma \Gamma_{\pi NN}^*(y, \mathbf{k}_T, \mathbf{p}_{2T}; \sigma, \sigma_2) \Gamma_{\pi NN}(y, \mathbf{k}_T, \mathbf{p}_{1T}; \sigma, \sigma_1) \quad (\sigma = \pm \frac{1}{2}). \quad (4.32)$$

In the last step we have expressed the bilinear forms in terms of the general  $\pi NN$  vertex function, which is regarded here as a function of the light-front momentum variables characterizing the on-shell nucleon 4-momenta. It is defined as

$$\Gamma_{\pi NN}(y, \mathbf{k}_T, \mathbf{p}_{1T}; \sigma, \sigma_1) \equiv -\frac{g_A}{2F_\pi} \bar{u}(l, \sigma) i \hat{k}_1 \gamma_5 u(p_1, \sigma_1), \quad (4.33)$$

where the light-front components of the nucleon 4-momenta  $p_1$  and  $l$  are given by [cf. Eq. (4.27)]

$$p_1^+ = p^+, \quad \mathbf{p}_{1T}, \quad p_1^- = \frac{|\mathbf{p}_{1T}|^2 + M_N^2}{p^+}, \quad (4.34)$$

$$l^+ = \bar{y}p^+, \quad \mathbf{l}_T = -\mathbf{k}_T, \quad l^- = \frac{|\mathbf{k}_T|^2 + M_N^2}{\bar{y}p^+}, \quad (4.35)$$

and the pion 4-momentum  $k_1$  is given by the difference of the nucleon 4-momenta,  $k_1 = p_1 - l$ , or

$$k_1^+ = yp^+, \quad \mathbf{k}_{1T} = \mathbf{p}_{1T} - \mathbf{l}_T, \quad k_1^- = p_1^- - l^-. \quad (4.36)$$

We emphasize that the assignment of the pion 4-momentum follows unambiguously from our reduction procedure. The second bilinear form in Eq. (4.31) is directly given by Eq. (4.33); the first bilinear form is given by the complex conjugate of the same function, evaluated at arguments  $\mathbf{p}_{1T} \rightarrow \mathbf{p}_{2T}$  and  $\sigma_1 \rightarrow \sigma_2$ . Because both nucleon 4-momenta at the  $\pi NN$  vertices are on mass shell, the vertices can equivalently be written as pseudoscalar vertices, cf. Eq. (3.21).

For the intermediate isobar contribution, using Eqs. (4.23) and (3.16), we get

$$A_{\Delta, \text{interm}} = -\frac{g_{\pi N \Delta}^2}{3M_N^2} [\bar{u}_2 k_{2\alpha} R^{\alpha\beta}(l) k_{1\beta} u_1]_{l^2=M_\Delta^2} \quad (4.37)$$

$$= -\frac{g_{\pi N \Delta}^2}{3M_N^2} \sum_\sigma [\bar{u}_2 k_{2\alpha} U^\alpha(l)] [\bar{U}^\beta(l) k_{1\beta} u_1] \quad (4.38)$$

$$= -\frac{2}{3} \sum_\sigma \Gamma_{\pi N \Delta}^*(y, \mathbf{k}_T, \mathbf{p}_{2T}; \sigma, \sigma_2) \Gamma_{\pi N \Delta}(y, \mathbf{k}_T, \mathbf{p}_{1T}; \sigma, \sigma_1) \quad (\sigma = \pm \frac{3}{2}, \pm \frac{1}{2}). \quad (4.39)$$

In the last step we have introduced the general vertex function for the  $\pi N \Delta$  transition, defined as

$$\Gamma_{\pi N \Delta}(y, \mathbf{k}_T, \mathbf{p}_{1T}; \sigma, \sigma_1) \equiv \frac{g_{\pi N \Delta}}{\sqrt{2}M_N} \bar{U}^\beta(l, \sigma) k_{1\beta} u(p_1, \sigma_1), \quad (4.40)$$

where the light-front components of the nucleon 4-momenta  $p_1$  and  $l$  are given by the same expressions as Eqs. (4.34) and (4.35), the only difference being that the minus component of the isobar momentum is

$$l^- = \frac{|\mathbf{k}_T|^2 + M_\Delta^2}{\bar{y}p^+}. \quad (4.41)$$

The pion 4-momentum  $k_1$  is again given by the difference of the baryon 4-momenta, Eq. (4.36).

In summary, the intermediate-baryon part of the peripheral current matrix element, Eq. (4.25), can be expressed as

$$\begin{aligned} \langle N_2 | J^+(0) | N_1 \rangle_{B, \text{interm}}^V &= \frac{p^+}{2\pi} \int_0^1 \frac{dy}{y\bar{y}} \int \frac{d^2 k_T}{(2\pi)^2} \\ &\times C_B \sum_\sigma \Psi_{N \rightarrow \pi B}^*(y, \mathbf{k}_T, \mathbf{p}_{2T}; \sigma, \sigma_2) \Psi_{N \rightarrow \pi B}(y, \mathbf{k}_T, \mathbf{p}_{1T}; \sigma, \sigma_1) \quad (B = N, \Delta), \end{aligned} \quad (4.42)$$

where

$$C_N = 2, \quad C_\Delta = -2/3 \quad (4.43)$$

are isospin factors, and

$$\Psi_{N \rightarrow \pi B}(y, \mathbf{k}_T, \mathbf{p}_{1T}; \sigma, \sigma_1) \equiv \frac{\Gamma_{\pi NB}(y, \mathbf{k}_T, \mathbf{p}_{1T}; \sigma, \sigma_1)}{\Delta \mathcal{M}_{N \rightarrow \pi B}^2(y, \mathbf{k}_T, \mathbf{p}_{1T})} \quad (4.44)$$

is the light-front wave function of the  $N \rightarrow \pi B$  transition, consisting of the vertex function and the invariant-mass denominator. Equation (4.42) represents the Feynman integral as an overlap integral of the light-front wave functions describing the transition from the initial nucleon state  $N_1$  to the  $\pi B$  intermediate state, and back to the final nucleon state  $N_2$ .

Some comments are in order regarding the isospin structure. In our convention the  $\pi NB$  vertex and the light-front wave function are normalized such that they describe the transition between the highest-isospin states of the initial nucleon and the intermediate baryon multiplets, which are

$$\begin{aligned} \text{intermediate } N: \quad p &\rightarrow p + \pi^0, \\ \text{intermediate } \Delta: \quad p &\rightarrow \Delta^{++} + \pi^-. \end{aligned} \quad (4.45)$$

The factors  $C_B$  account for the total contribution of configurations with an intermediate baryon and pion to the nucleon's isovector current, including the probability for the configuration (i.e., the square of the coupling constant) and the pion charge. To determine the values, let us assume that the external nucleon state is the proton. In the case of intermediate  $N$ , the only configuration contributing to the current is  $n + \pi^+$  (with relative coupling  $\sqrt{2}$ ), and the isospin factor is  $C_N = \sqrt{2} \times \sqrt{2} = 2$ . In the case of intermediate  $\Delta$ , the possible configurations are  $\Delta^{++} + \pi^-$  (with relative coupling 1) and  $\Delta^0 + \pi^+$  (with relative coupling  $1/\sqrt{3}$ ), and the isospin factor is  $C_\Delta = (-1 + \frac{1}{3})/(-1) = \frac{2}{3}$ .

The light-front wave functions of the nucleons moving with transverse momenta  $\mathbf{p}_{1T}$  and  $\mathbf{p}_{2T}$  can be expressed in terms of those in the transverse rest frame [8]. The relation between the wave functions follows from the Lorentz invariance of the vertex function and the invariant-mass denominator and takes the form

$$\Psi_{N \rightarrow \pi B}(y, \mathbf{k}_T, \mathbf{p}_{1T}; \sigma, \sigma_1) = \Psi(y, \mathbf{k}_T + \bar{y}\mathbf{p}_{1T}, \mathbf{0}; \sigma, \sigma_1) \equiv \Psi(y, \mathbf{k}_T + \bar{y}\mathbf{p}_{1T}; \sigma, \sigma_1). \quad (4.46)$$

For simplicity we denote the light-front wave function in the transverse rest frame by the same symbol as that of the moving nucleon, only dropping the overall transverse momentum argument. The explicit expressions for the rest frame wave function can be obtained by setting  $\mathbf{p}_{1T} = 0$  in the invariant mass difference Eq. (4.29) and the vertices, Eqs. (4.33) and (4.40). They are:

$$\Psi_{N \rightarrow \pi B}(y, \tilde{\mathbf{k}}_T; \sigma, \sigma_1) \equiv \frac{\Gamma_{\pi NB}(y, \tilde{\mathbf{k}}_T; \sigma, \sigma_1)}{\Delta \mathcal{M}_{N \rightarrow \pi B}^2(y, \tilde{\mathbf{k}}_T)} \quad (B = N, \Delta), \quad (4.47)$$

$$\Delta \mathcal{M}_{N \rightarrow \pi B}^2(y, \tilde{\mathbf{k}}_T) \equiv \frac{\tilde{\mathbf{k}}_T^2 + M_\pi^2}{y} + \frac{\tilde{\mathbf{k}}_T^2 + M_B^2}{\bar{y}} - M_N^2, \quad (4.48)$$

$$\Gamma_{\pi NN}(y, \tilde{\mathbf{k}}_T; \sigma, \sigma_1) \equiv -\frac{g_A}{2F_\pi} \bar{u}(l, \sigma) i(\hat{p}_1 - \hat{l}) \gamma_5 u(p_1, \sigma_1), \quad (4.49)$$

$$\Gamma_{\pi N\Delta}(y, \tilde{\mathbf{k}}_T; \sigma, \sigma_1) \equiv \frac{g_{\pi N\Delta}}{\sqrt{2}M_N} \bar{U}^\mu(l, \sigma)(p_1 - l)_\mu u(p_1, \sigma_1), \quad (4.50)$$

$$p_1^+ = p^+, \quad \mathbf{p}_{1T} = 0, \quad p_1^- = \frac{M_N^2}{p^+}, \quad (4.51)$$

$$l^+ = \bar{y}p^+, \quad \mathbf{l}_T = -\tilde{\mathbf{k}}_T, \quad l^- = \frac{|\tilde{\mathbf{k}}_T|^2 + M_B^2}{\bar{y}p^+}, \quad (4.52)$$

where  $\tilde{\mathbf{k}}_T$  denotes the transverse momentum argument of the rest frame wave function (see Fig. 4). In terms of the rest-frame wave functions the peripheral current matrix element is then given by

$$\begin{aligned} \langle N_2 | J^+(0) | N_1 \rangle_{B, \text{interm}}^V &= \frac{p^+}{2\pi} \int_0^1 \frac{dy}{y\bar{y}} \int \frac{d^2k_T}{(2\pi)^2} \\ &\times C_B \sum_\sigma \Psi_{N \rightarrow \pi B}^*(y, \mathbf{k}_T + \bar{y}\mathbf{p}_{2T}; \sigma, \sigma_2) \Psi_{N \rightarrow \pi B}(y, \mathbf{k}_T + \bar{y}\mathbf{p}_{1T}; \sigma, \sigma_1) \quad (B = N, \Delta). \end{aligned} \quad (4.53)$$

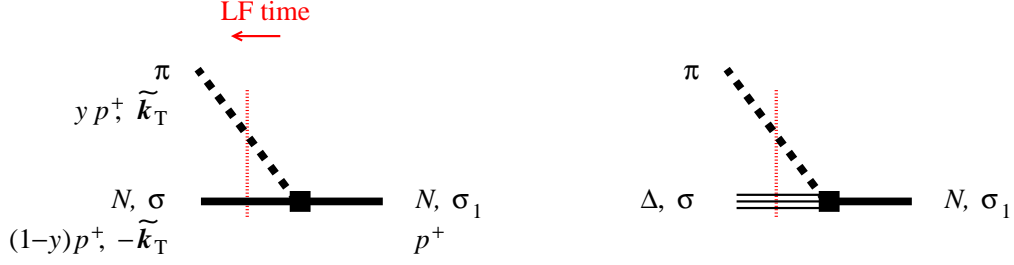


FIG. 4. Light-front wave functions of  $N \rightarrow \pi B$  transition in chiral EFT ( $B = N, \Delta$ ). The spin quantum number and the light-front momenta of the particles are indicated. The transverse momenta correspond to the transverse rest frame, Eq. (4.47).

### C. Polarization states

To evaluate the wave function overlap formulas we need to specify the polarization states for the nucleon and isobar spinors. It is natural to describe the polarization of the particles using light-front helicity states [28]. In this formulation one constructs the spinor/vector for a particle with light-front momentum  $l^+$  and  $\mathbf{l}_T$  by starting with the spinor/vector in the particle rest frame ( $l^+ = M_B, \mathbf{l}_T = 0$ ), then performing a longitudinal boost to the desired longitudinal momentum  $l^+ \neq M_B$ , then a transverse boost to  $\mathbf{l}_T \neq 0$ . The spinors/vectors thus defined correspond to definite polarization states in the particle rest frame and transform in a simple way under longitudinal and transverse boosts.

The bispinors for a spin-1/2 particle of mass  $M_B$  with definite light-front helicity  $\sigma = \pm 1/2$  are given explicitly by [27, 28]

$$u(l, \sigma) = \frac{1}{\sqrt{2l^+}} [l^+ \gamma^- + (M_B - \boldsymbol{\gamma}_T \cdot \mathbf{l}_T) \gamma^+] \begin{pmatrix} \chi(\sigma) \\ 0 \end{pmatrix}, \quad (4.54)$$

where  $\chi(\sigma)$  are the rest-frame 2-spinors for polarization in the positive and negative  $z$ -direction,

$$\chi(\sigma = 1/2) = \begin{pmatrix} 1 \\ 0 \end{pmatrix}, \quad \chi(\sigma = -1/2) = \begin{pmatrix} 0 \\ 1 \end{pmatrix}. \quad (4.55)$$

The bispinors Eq. (4.54) satisfy the normalization and completeness relations, Eqs. (3.2) and (3.4) for the nucleon ( $B = N$ ), or Eqs. (3.10) and (3.11) for the isobar ( $B = \Delta$ ). Similarly, the polarization vectors for a spin-1 particle with definite light-front helicity  $\lambda = (1, 0, -1)$  are given by (see e.g. Ref. [35])

$$\begin{aligned} \epsilon^+(\lambda, l) &= \frac{l^+}{M_\Delta} \alpha^z(\lambda), \\ \epsilon^-(\lambda, l) &= \frac{l_T^2 - M_\Delta^2}{M_\Delta l^+} \alpha^z(\lambda) + \frac{2\mathbf{l}_T}{l_+} \cdot \boldsymbol{\alpha}_T(\lambda), \\ \boldsymbol{\epsilon}_T(\lambda, l) &= \frac{\mathbf{l}_T}{M_\Delta} \alpha^z(\lambda) + \boldsymbol{\alpha}_T(\lambda), \end{aligned} \quad (4.56)$$

where  $\boldsymbol{\alpha}(\lambda) \equiv (\alpha^z(\lambda), \boldsymbol{\alpha}_T(\lambda))$  denotes the polarization 3-vector of the particle in the rest frame,

$$\boldsymbol{\epsilon}(\lambda, l) = (0, \boldsymbol{\alpha}(\lambda)) \quad [\text{rest frame, } l = (M_\Delta, 0)], \quad (4.57)$$

and describes states with circular polarization along the  $z$ -axis,

$$\boldsymbol{\alpha}(\lambda = \pm 1) = \frac{1}{\sqrt{2}} \begin{pmatrix} \mp 1 \\ -i \\ 0 \end{pmatrix}, \quad \boldsymbol{\alpha}(\lambda = 0) = \begin{pmatrix} 0 \\ 0 \\ 1 \end{pmatrix}. \quad (4.58)$$

The vector-bispinors for a spin-3/2 particle with definite light-front helicity are then defined by Eq. (3.5). The coupling of the spinors to spin-3/2 is performed in rest frame, and the bispinor and vector are boosted independently to the desired light-front momentum.

Using the light-front helicity spinors we can now compute the components of the  $\pi NB$  vertex function in the nucleon rest frame. The results are conveniently expressed as bilinear forms between the rest-frame spinors/vectors characterizing the states. For the transition to a nucleon ( $B = N$ ) we obtain from Eq. (4.49)

$$\Gamma_{\pi NN}(y, \tilde{\mathbf{k}}_T; \sigma, \sigma_1) = \frac{2ig_A M_N}{F_\pi \sqrt{y}} \left[ y M_N S^z(\sigma, \sigma_1) + \tilde{\mathbf{k}}_T \cdot \mathbf{S}_T(\sigma, \sigma_1) \right], \quad (4.59)$$

where  $S^z$  and  $\mathbf{S}_T \equiv (S^x, S^y)$  are the components of the 3-vector characterizing the spin transition matrix element in the rest frame

$$S^i(\sigma, \sigma_1) \equiv \chi^\dagger(\sigma) (\frac{1}{2} \sigma^i) \chi(\sigma_1) \quad (i = x, y, z), \quad (4.60)$$

in which  $\sigma^i$  are the Pauli matrices. The first term in Eq. (4.59) is diagonal in the nucleon light-front helicity,  $S^z(\sigma, \sigma_1) = \sigma \delta(\sigma, \sigma_1)$ , and describes a transition to a  $\pi N$  state with orbital angular momentum projection  $L^z = 0$ . The second term in Eq. (4.59) is off-diagonal in light-front helicity and describes a transition to a state in which the pion has orbital angular momentum projection  $L^z = \pm 1$ . For the transition to the isobar ( $B = \Delta$ ) the vertex given by Eq. (4.50) can be written as

$$\Gamma_{\pi N \Delta}(y, \tilde{\mathbf{k}}_T; \sigma, \sigma_1) = \sum_{\lambda \sigma'} C_{1, \lambda; 1/2, \sigma'}^{3/2, \sigma} \boldsymbol{\alpha}(\lambda) \cdot \mathcal{P}(y, \tilde{\mathbf{k}}_T, \sigma', \sigma_1), \quad (4.61)$$

where the 3-vector  $\mathcal{P} \equiv (\mathcal{P}^z, \mathcal{P}_T)$  represents the bilinear form in the bispinors in the vertex function. Its components are obtained as

$$\left. \begin{array}{l} \mathcal{P}^z \\ \mathcal{P}_T \end{array} \right\} (y, \tilde{\mathbf{k}}_T, \sigma', \sigma_1) = \frac{\sqrt{2} g_{\pi N \Delta}}{M_N \bar{y}^{3/2}} \left\{ \bar{M} \delta(\sigma', \sigma_1) + i \tilde{\mathbf{k}}_T \cdot [\mathbf{e}_z \times \mathbf{S}_T(\sigma', \sigma_1)] \right\} \left\{ \begin{array}{l} \frac{\tilde{\mathbf{k}}_T^2}{2M_\Delta} - M_d \\ -\tilde{\mathbf{k}}_T \end{array} \right\}, \quad (4.62)$$

in which

$$\bar{M} \equiv \frac{M_\Delta + \bar{y} M_N}{2}, \quad (4.63)$$

$$M_d \equiv \frac{M_\Delta^2 - \bar{y}^2 M_N^2}{2M_\Delta}. \quad (4.64)$$

#### D. Coordinate-space wave function

The peripheral transverse densities are conveniently expressed in terms of the transverse coordinate-space wave functions of the  $N \rightarrow \pi B$  transition. They are defined as the transverse Fourier transform of the momentum-space wave functions at fixed longitudinal momentum fraction  $y$ ,

$$\Phi_{N \rightarrow \pi B}(y, \mathbf{r}_T, \sigma, \sigma_1) \equiv \int \frac{d^2 \tilde{\mathbf{k}}_T}{(2\pi)^2} e^{i \tilde{\mathbf{k}}_T \cdot \mathbf{r}_T} \Psi_{N \rightarrow \pi B}(y, \tilde{\mathbf{k}}_T; \sigma, \sigma_1) \quad (4.65)$$

$$= \int \frac{d^2 \tilde{\mathbf{k}}_T}{(2\pi)^2} e^{i \tilde{\mathbf{k}}_T \cdot \mathbf{r}_T} \frac{\Gamma_{\pi NB}(y, \tilde{\mathbf{k}}_T; \sigma, \sigma_1)}{\Delta \mathcal{M}_{N \rightarrow \pi B}^2(y, \tilde{\mathbf{k}}_T)}. \quad (4.66)$$

The vector  $\mathbf{r}_T$  represents the relative transverse coordinate, i.e., the difference of the transverse positions of the  $\pi$  and  $B$ , which are regarded as point particles in the context of chiral EFT. The wave function thus describes the physical transverse size distribution of the  $\pi B$  system in the intermediate state. The invariant-mass denominator in Eq. (4.66) is given by Eq. (4.48) and can be written in the form

$$\Delta \mathcal{M}_{N \rightarrow \pi B}^2(y, \tilde{\mathbf{k}}_T) = \frac{\tilde{\mathbf{k}}_T^2 + M_{T,B}^2}{y \bar{y}}, \quad (4.67)$$

where  $M_{T,B} \equiv M_{T,B}(y)$  is the  $y$ -dependent transverse mass governing the transverse momentum dependence,

$$\begin{aligned} M_{T,B}^2 &\equiv \bar{y} M_\pi^2 + y (M_B^2 - \bar{y} M_N^2) \\ &= \bar{y} M_\pi^2 + y^2 M_N^2 + y (M_B^2 - M_N^2). \end{aligned} \quad (4.68)$$

The Fourier transform Eq. (4.66) can be expressed in terms of modified Bessel functions using the identity

$$\int \frac{d^2 \tilde{\mathbf{k}}_T}{(2\pi)^2} \frac{e^{i\mathbf{r}_T \cdot \tilde{\mathbf{k}}_T}}{\tilde{\mathbf{k}}_T^2 + M_{T,B}^2} = \frac{K_0(M_{T,B} r_T)}{2\pi} \quad (r_T \equiv |\mathbf{r}_T|), \quad (4.69)$$

from which formulas with additional powers of  $\tilde{\mathbf{k}}_T$  in the numerator can be derived by differentiating with respect to the vector  $\mathbf{r}_T$ . The coordinate-space wave functions can be represented as sums of spin structures depending on the transverse unit vector  $\mathbf{n}_T \equiv \mathbf{r}_T/r_T$ , multiplied by radial functions depending on the modulus  $r_T$ .

For the nucleon intermediate state ( $B = N$ ) the coordinate-space wave function is of the form [8]

$$\Phi_{N \rightarrow \pi N}(y, \mathbf{r}_T, \sigma, \sigma_1) = -2iS^z(\sigma, \sigma_1) U_0(y, r_T) + 2\mathbf{n}_T \cdot \mathbf{S}_T(\sigma, \sigma_1) U_1(y, r_T) \quad (\mathbf{n}_T \equiv \mathbf{r}_T/r_T). \quad (4.70)$$

The two terms in Eq. (4.70) represent structures with definite orbital angular momentum around the  $z$ -axis in the rest frame, namely  $L^z = 0$  and  $L^z = \pm 1$ . The radial wave functions are obtained as

$$\left. \begin{array}{l} U_0(y, r_T) \\ U_1(y, r_T) \end{array} \right\} = \frac{g_A M_N y \sqrt{y}}{2\pi F_\pi} \left\{ \begin{array}{l} y M_N K_0(M_{T,N} r_T) \\ M_{T,N} K_1(M_{T,N} r_T) \end{array} \right\}. \quad (4.71)$$

For the isobar intermediate state ( $B = \Delta$ ) the coordinate-space wave function is of the form

$$\Phi_{N \rightarrow \pi \Delta}(y, \mathbf{r}_T, \sigma, \sigma_1) = \sum_{\lambda \sigma'} C_{1,\lambda; 1/2,\sigma'}^{3/2,\sigma} \boldsymbol{\alpha}(\lambda) \cdot \boldsymbol{\mathcal{R}}(y, \mathbf{r}_T, \sigma', \sigma_1), \quad (4.72)$$

where  $\boldsymbol{\mathcal{R}} \equiv (\mathcal{R}^z, \boldsymbol{\mathcal{R}}_T)$  is a 3-vector-valued function, the components of which are given by

$$\mathcal{R}^z(y, \mathbf{r}_T, \sigma', \sigma_1) = -V_0(y, r_T) \delta + 2\mathbf{n}_T \cdot (\mathbf{e}_z \times \mathbf{S}_T) V_1(y, r_T), \quad (4.73)$$

$$\begin{aligned} \boldsymbol{\mathcal{R}}_T(y, \mathbf{r}_T, \sigma', \sigma_1) = & -2i(\mathbf{e}_z \times \mathbf{S}_T) W_0(y, r_T) - i\mathbf{n}_T W_1(y, r_T) \delta - 2i(\mathbf{n}_T \otimes \mathbf{n}_T - \frac{1}{2}\mathbf{1}) \cdot (\mathbf{e}_z \times \mathbf{S}_T) W_2(y, r_T) \\ & [\mathbf{n}_T \equiv \mathbf{r}_T/r_T, \delta \equiv \delta(\sigma', \sigma_1), \mathbf{S}_T \equiv \mathbf{S}_T(\sigma', \sigma_1)]. \end{aligned} \quad (4.74)$$

$\mathcal{R}^z$  contains structures with orbital angular momentum  $L^z = 0$  and  $\pm 1$ , whereas  $\boldsymbol{\mathcal{R}}_T$  contains structures with  $L^z = 0, \pm 1$  and  $\pm 2$ . The radial functions are now obtained as

$$\left. \begin{array}{l} V_0 \\ V_1 \\ W_0 \\ W_1 \\ W_2 \end{array} \right\} (y, r_T) = \frac{g_{\pi N \Delta} y}{2\pi \sqrt{2} M_N \sqrt{y}} \left\{ \begin{array}{l} 2\bar{M} \left( \frac{M_{T\Delta}^2}{2M_\Delta} + M_d \right) K_0(M_{T\Delta} r_T) \\ M_{T\Delta} \left( \frac{M_{T\Delta}^2}{2M_\Delta} + M_d \right) K_1(M_{T\Delta} r_T) \\ \frac{1}{2} M_{T\Delta}^2 K_0(M_{T\Delta} r_T) \\ 2\bar{M} M_{T\Delta} K_1(M_{T\Delta} r_T) \\ M_{T\Delta}^2 K_2(M_{T\Delta} r_T) \end{array} \right\}. \quad (4.75)$$

The coordinate-space wave functions fall off exponentially at large transverse distances  $r_T$ , with a width that is determined by the inverse transverse mass Eq. (4.68) and depends on the pion momentum fraction  $y$ . At large values of the argument the modified Bessel functions behave as

$$K_n(M_{T,B} r_T) \sim \sqrt{\frac{\pi}{2}} \frac{e^{-M_{T,B} r_T}}{\sqrt{M_{T,B} r_T}} \quad (M_{T,B} r_T \gg 1; n = 0, 1, 2, \dots). \quad (4.76)$$

This behavior is caused by the singularity of the momentum-space wave function at (complex) transverse momenta  $\tilde{\mathbf{k}}_T^2 = -M_{T,B}^2$ , cf. Eq. (4.67), which corresponds to the vanishing of the invariant mass denominator of the wave function,  $\Delta \mathcal{M}^2 = 0$ .

The chiral  $N \rightarrow \pi B$  light-front wave functions are defined in the parametric domain

$$y = O(M_\pi/M_N), \quad |\mathbf{r}_T| = O(M_\pi^{-1}), \quad \text{or} \quad |\tilde{\mathbf{k}}_T| = O(M_\pi), \quad (4.77)$$

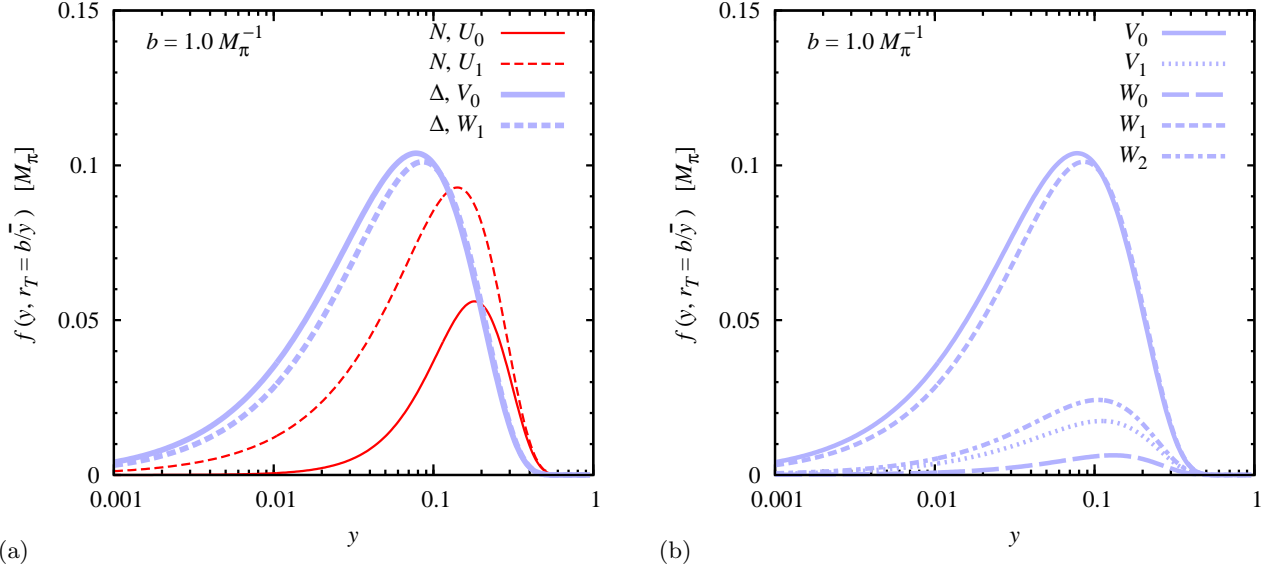


FIG. 5. Chiral light-front wave functions in coordinate representation. (a) Radial wave functions of  $\pi N$  system ( $U_0, U_1$ ) and  $\pi\Delta$  system (dominant  $V_0, W_1$ ), as functions of the pion momentum fraction  $y$ , at transverse separation  $r_T = b/\sqrt{y}$  with  $b = 1.0 M_\pi^{-1}$ . (b) Full set of radial wave functions of  $\pi\Delta$  system.

where they describe peripheral pions carrying a parametrically small fraction of the nucleon's longitudinal momentum, and are to be used in this domain only. In the nucleon rest frame this corresponds to the domain in which all components of the pion 4-momentum are  $O(M_\pi)$  (“soft pion”) and chiral dynamics is valid. In the case of the nucleon intermediate state ( $B = N$ ), Eq. (4.68) shows that for  $y = O(M_\pi/M_N)$  the transverse mass is

$$M_{T,N} = O(M_\pi) \quad \text{for} \quad y = O(M_\pi/M_N), \quad (4.78)$$

so that the exponential range of the coordinate-space wave function is  $O(M_\pi^{-1})$ , cf. Eq. (4.76). In the case of the isobar intermediate state ( $B = \Delta$ ) the situation is more complex, as an additional scale is present in the  $N$ - $\Delta$  mass splitting. The transverse mass squared Eq. (4.68) now contains a term

$$y(M_\Delta^2 - M_N^2) = y(M_\Delta - M_N)(M_\Delta + M_N), \quad (4.79)$$

which is of “mixed” order  $O[M_\pi(M_\Delta - M_N)]$  for regular chiral momentum fractions  $y = O(M_\pi/M_N)$ , and becomes  $O(M_\pi^2)$  only for parametrically small fractions  $y = O\{M_\pi^2/[(M_\Delta - M_N)M_N]\}$ . In the strict chiral limit  $M_\pi \rightarrow 0$  at fixed  $M_\Delta - M_N$  the isobar intermediate state would therefore be a short-distance contribution to the densities, or parametrically suppressed at distances  $O(M_\pi^{-1})$ . However, at the physical value of  $M_\pi$  the  $O[M_\pi(M_\Delta - M_N)]$  term in Eq. (4.68) is numerically of the same magnitude as the  $O(M_\pi^2)$  ones, and the intermediate isobar contribution is comparable to the intermediate nucleon one, as is seen in the numerical results below (see Fig. 5a).

For pion longitudinal momentum fractions  $y = O(1)$  the transverse mass Eq. (4.68) is  $M_T = O(M_B)$  for both  $B = N$  and  $\Delta$  intermediate states, and the transverse range of the wave functions is  $O(M_B^{-1})$ . This region does not correspond to chiral dynamics, and the wave functions defined by the above expressions have no physical meaning there. In the calculation of the peripheral transverse densities this region of  $y$  does not contribute, as the wave functions will be evaluated at distances  $r_T = b/(1-y)$  and therefore vanish exponentially in the limit  $y \rightarrow 1$ , cf. Eq. (4.76). In the calculations in Sec. II we can thus formally extend the integral up to  $y = 1$  without violating the parametric restriction Eq. (4.77). This self-regulating property is a major advantage of our coordinate-space formulation. The selection of large transverse distances  $b = O(M_\pi^{-1})$  automatically enforces the parametric restrictions in the wave function overlap integral, and no explicit regulators are required.<sup>2</sup>

Numerical results for the  $N \rightarrow \pi B$  wave functions are shown in Figs. 5a and b. Figure 5a shows the radial functions for the intermediate nucleon,  $U_0$  and  $U_1$ , and the two dominant radial functions for the isobar,  $V_0$  and

<sup>2</sup> The intermediate isobar wave functions Eq. (4.75) contain a prefactor  $1/\sqrt{y}$  and become infinite when taking the limit  $y \rightarrow 1$  at fixed separation  $r_T$ . This singularity is purely formal and occurs outside of the parametric region of applicability. In the calculation of the transverse densities the wave functions are evaluated at moving separation  $r_T = b/\sqrt{y}$  and vanish exponentially in the limit  $y \rightarrow 1$ , cf. Eq. (4.76) and Figs. 5a and b.

$W_1$ , as functions of the pion longitudinal momentum fraction  $y$ . The functions are evaluated at a moving transverse separation  $r_T = b/\bar{y}$ , in the same way as they enter in the calculation of the transverse densities (see Sec. IV E). Several features are worth noting: (a) The nucleon radial functions are centered around values  $y \sim M_\pi/M_N$ . The isobar wave functions are shifted toward slightly smaller  $y$ , due to the different behavior of the transverse mass. (b) The radial functions at fixed  $b$  vanish exponentially for  $y \rightarrow 1$ . (c) The helicity-conserving ( $L^z = 0$ ) nucleon function  $U_0$  and the helicity-flip ( $L^z = 1$ ) function  $U_1$  are of the same magnitude at non-exceptional  $y$ . In the limit  $y \rightarrow 1$  the two functions approach each other; in the limit  $y \rightarrow 0$  the helicity-conserving function vanishes more rapidly than the helicity-flip one. The same pattern is observed for the helicity-conserving and -flip isobar wave functions,  $V_0$  and  $W_1$ . (d) Intermediate nucleon and isobar wave functions are generally of the same magnitude.

Figure 5a shows the full set of radial wave functions for the intermediate isobar, Eq. (4.75). It is seen that the functions  $V_0$  and  $W_1$  are numerically dominant over  $V_1, W_0$  and  $W_2$ . This pattern follows from the fact that  $\bar{M} \gg M_{T,\Delta}$  at non-exceptional values of  $y$  and can be explained more formally in the large- $N_c$  limit (see Sec. VI).

### E. Peripheral densities

The final step now is to calculate the peripheral transverse densities in terms of the coordinate-space light-front wave functions [8]. To this end we consider the general form factor decomposition of current matrix element Eq. (2.1) in the frame where momentum transfer  $\Delta$  is transverse, Eq. (4.27), and with the nucleon spin states chosen as light-front helicity states Eq. (4.54),

$$\begin{aligned} \langle N_2 | J^+(0) | N_1 \rangle &\equiv \langle N(p^+, \mathbf{p}_{2T}, \sigma_2) | J^+(0) | N(p^+, \mathbf{p}_{1T}, \sigma_1) \rangle \\ &= 2p^+ \left[ \delta(\sigma_2, \sigma_1) F_1(-\Delta_T^2) - i(\mathbf{e}_z \times \Delta_T) \cdot \mathbf{S}_T(\sigma_2, \sigma_1) \frac{F_2(-\Delta_T^2)}{M_N} \right]. \end{aligned} \quad (4.80)$$

The spin vector  $\mathbf{S}_T(\sigma_2, \sigma_1)$  here is defined as in Eq. (4.60), but with the rest-frame 2-spinors describing the initial and final nucleon. The term containing the form factor  $F_1$  is diagonal in the nucleon light-front helicity, while the term with  $F_2$  is off-diagonal. Explicit expressions for the form factors  $F_1$  and  $F_2$  are thus obtained by taking the diagonal and off-diagonal light-front helicity components, or, more conveniently, by multiplying Eq. (4.80) with  $\delta(\sigma_1, \sigma_2)$  and  $(\mathbf{e}_z \times \Delta_T) \cdot \mathbf{S}_T(\sigma_1, \sigma_2)$  and summing over  $\sigma_1$  and  $\sigma_2$ ,

$$\left. \begin{array}{l} F_1(-\Delta_T^2) \\ F_2(-\Delta_T^2) \end{array} \right\} = \frac{1}{2p^+} \sum_{\sigma_1 \sigma_2} \langle N_2 | J^+(0) | N_1 \rangle \left\{ \begin{array}{l} \frac{1}{2} \delta(\sigma_1, \sigma_2) \\ \frac{2M_N}{\Delta_T^2} i(\mathbf{e}_z \times \Delta_T) \cdot \mathbf{S}_T(\sigma_1, \sigma_2) \end{array} \right\}. \quad (4.81)$$

The peripheral current matrix element is expressed as an overlap integral of the momentum-space  $N \rightarrow \pi B$  light-front wave functions in Eq. (4.53). In terms of the coordinate-space wave functions it becomes ( $B = N, \Delta$ )

$$\langle N_2 | J^+(0) | N_1 \rangle_{B, \text{interm}}^V = \frac{p^+}{2\pi} \int_0^1 \frac{dy}{y\bar{y}} \int d^2 r_T e^{i\bar{y} r_T \Delta_T} C_B \sum_{\sigma} \Phi_{N \rightarrow \pi B}^*(y, \mathbf{r}_T; \sigma, \sigma_2) \Phi_{N \rightarrow \pi B}(y, \mathbf{r}_T; \sigma, \sigma_1). \quad (4.82)$$

Note that the momentum transfer  $\Delta_T$  is Fourier-conjugate to  $\bar{y} r_T$ ; this follows from the particular shift in the arguments of the rest-frame momentum-space wave functions and is a general feature of light-front kinematics. Substituting Eq. (4.82) in Eq. (4.81) and calculating the Fourier transform according to Eq. (2.5), we obtain the intermediate-baryon contribution to the transverse densities<sup>3</sup> ( $B = N, \Delta$ )

$$\left. \begin{array}{l} \rho_{1,B}^V(b) \\ (\mathbf{e}_z \times \mathbf{n}_T) \tilde{\rho}_{2,B}^V(b) \end{array} \right\} = \frac{C_B}{4\pi} \int_0^1 \frac{dy}{y\bar{y}^3} \sum_{\sigma_1, \sigma_2, \sigma} \Phi_{N \rightarrow \pi B}^*(y, \mathbf{r}_T; \sigma, \sigma_2) \Phi_{N \rightarrow \pi B}(y, \mathbf{r}_T; \sigma, \sigma_1) \left\{ \begin{array}{l} \frac{1}{2} \delta(\sigma_1, \sigma_2) \\ \mathbf{S}_T(\sigma_1, \sigma_2) \end{array} \right\} \quad (4.83)$$

$$(\mathbf{n}_T = \mathbf{b}/|\mathbf{b}|, \mathbf{r}_T = \mathbf{b}/\bar{y}).$$

In the representation Eq. (4.83) transverse rotational invariance is not manifest; however, the densities are in fact rotationally invariant, as the angular factors are compensated by the angular dependence of wave function. Specifically,

<sup>3</sup> For ease of notation we omit the label ‘‘interm’’ on the intermediate-baryon contribution to the densities and agree that  $\rho_{1,B}^V(b) \equiv \rho_{1,B}^V(b)_{\text{interm}}$  in the following. Explicit labels ‘‘interm’’ and ‘‘cont’’ will be used in Sec. VI, where we include the contact term contribution.

if we project the equation for the spin-dependent density on the  $y$ -direction, it becomes

$$\cos \phi \tilde{\rho}_2^V(b) = \frac{C_B}{4\pi} \int_0^1 \frac{dy}{y\bar{y}^3} \sum_{\sigma_1, \sigma_2, \sigma} \Phi_{N \rightarrow \pi B}^*(y, \mathbf{r}_T; \sigma, \sigma_2) \Phi_{N \rightarrow \pi B}(y, \mathbf{r}_T; \sigma, \sigma_1) S^y(\sigma_1, \sigma_2) \quad (4.84)$$

$$(\mathbf{r}_T = \mathbf{b}/\bar{y}),$$

in accordance with Eq. (2.6) and the visualization in Fig. 1a. Note that the expressions in Eqs. (4.83) and (4.84) are diagonal in the pion longitudinal momentum fraction  $y$  and the transverse separation  $\mathbf{r}_T$ , and thus represent true densities of the light-front wave functions of the intermediate  $\pi B$  systems [2, 4, 5].

We can now express the transverse densities in terms of the radial wave functions, by substituting in Eqs. (4.83) and (4.84) the explicit form of the coordinate-space wave functions, Eqs. (4.70) and (4.72), and performing the spin sums. The intermediate nucleon and isobar contributions are obtained as

$$\left. \begin{array}{l} \rho_{1,N}^V(b) \\ \tilde{\rho}_{2,N}^V(b) \end{array} \right\} = \frac{C_N}{4\pi} \int_0^1 \frac{dy}{y\bar{y}^3} \left\{ \begin{array}{l} U_0^2 + U_1^2 \\ -2U_0U_1 \end{array} \right\}, \quad (4.85)$$

$$\left. \begin{array}{l} \rho_{1,\Delta}^V(b) \\ \tilde{\rho}_{2,\Delta}^V(b) \end{array} \right\} = \frac{C_\Delta}{6\pi} \int \frac{dy}{y\bar{y}^3} \left\{ \begin{array}{l} (V_0 + W_0)^2 + (V_1 + \frac{1}{2}W_1)^2 + \frac{3}{4}(W_1^2 + W_2^2) \\ 2(V_0 + W_0)(V_1 + \frac{1}{2}W_1) + \frac{3}{2}W_1W_2 \end{array} \right\} \quad (4.86)$$

$$[U_0 \equiv U_0(y, r_T = b/\bar{y}), \text{ etc.}].$$

Two properties of these expressions are worth noting: (a) Rotational invariance of the densities is now manifest, as the angular-dependent factors have canceled in the calculation. (b) The spin-independent density  $\rho_{1,B}^V$  involves products of functions with the same orbital angular momentum, while the spin-dependent density  $\tilde{\rho}_{2,B}^V$  involves products of functions differing by one unit of angular momentum; i.e., one has the selection rules ( $B = N, \Delta$ )

$$\left. \begin{array}{l} \rho_{1,B}^V : \quad \Delta L^z = 0 \\ \tilde{\rho}_{2,B}^V : \quad \Delta L^z = 1 \end{array} \right\}. \quad (4.87)$$

This appears natural in view of the light-front helicity structure of the form factors, Eq.(4.81).

The left and right current densities, Eq. (2.8), are readily obtained as the sum and difference of the spin-independent and -dependent densities in Eqs. (4.85) and (4.86),

$$\rho_{\text{left/right},N}^V(b) = \rho_{1,N}^V \mp \tilde{\rho}_{2,N}^V = \frac{C_N}{4\pi} \int \frac{dy}{y\bar{y}^3} (U_0 \pm U_1)^2, \quad (4.88)$$

$$\rho_{\text{left/right},\Delta}^V(b) = \rho_{1,\Delta}^V \mp \tilde{\rho}_{2,\Delta}^V = \frac{C_\Delta}{6\pi} \int \frac{dy}{y\bar{y}^3} [(V_0 + W_0 \mp V_1 \mp \frac{1}{2}W_1)^2 + \frac{3}{4}(W_1 \mp W_2)^2] \quad (4.89)$$

$$[U_0 \equiv U_0(y, r_T = b/\bar{y}), \text{ etc.}].$$

The integrands in both expressions are explicitly positive. Taking into account the signs of the isospin factors, Eq. (4.43), we conclude that

$$\rho_{\text{left/right},N}^V(b) > 0, \quad (4.90)$$

$$\rho_{\text{left/right},\Delta}^V(b) < 0. \quad (4.91)$$

This generalizes the positivity condition for the intermediate-nucleon contribution derived in Ref. [8]. The definiteness conditions Eqs. (4.90) and (4.91) represent new insights into the structure of the transverse densities gained from the light-front representation, as they rely essentially on the expression of the densities as quadratic forms in the wave function. The conditions are essential for the quantum-mechanical interpretation of the transverse densities as the current carried by a quasi-free peripheral pion (see Sec. V).

We can now evaluate the densities numerically using the overlap formulas. Figure 6a shows the integrand of the spin-independent and -dependent densities as a function of  $y$ , at a typical chiral distance  $b = 1.0 M_\pi^{-1}$ . One observes that: (a) The intermediate nucleon contributes positively to  $\rho_1^V$  and negatively to  $\tilde{\rho}_2^V$ , while the intermediate isobar

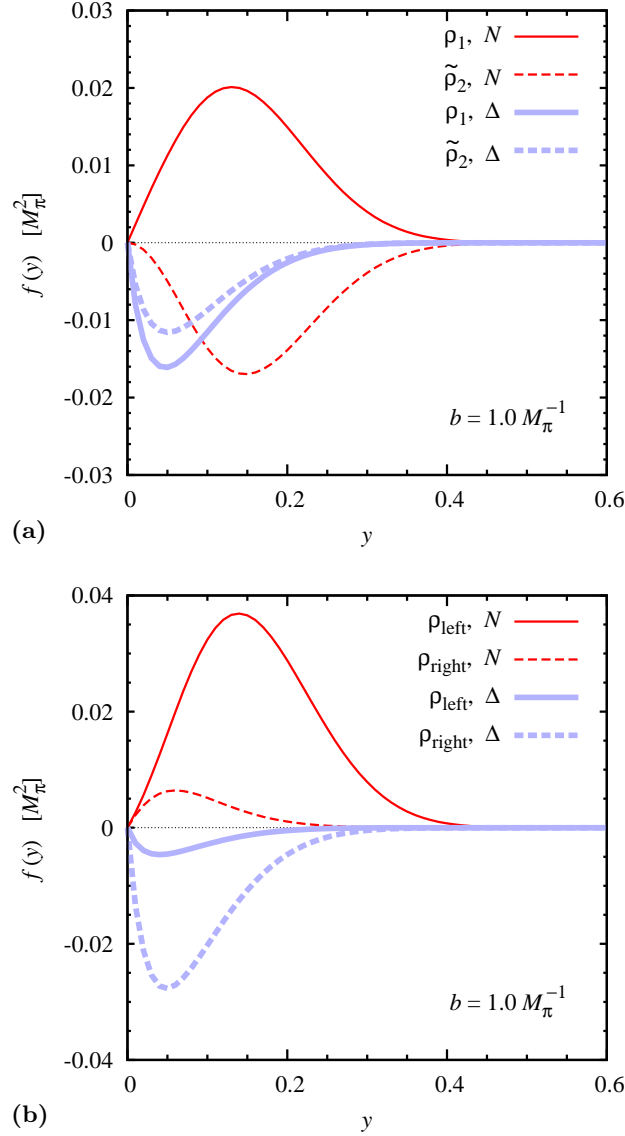


FIG. 6. Integrands of the light-front wave function overlap integrals for the peripheral transverse densities, as functions of the pion momentum fraction  $y$ , at a distance  $b = 1.0 M_\pi^{-1}$ . (a) Integrands of the  $N$  and  $\Delta$  contributions to the spin-independent and -dependent densities,  $\rho_1^V$  and  $\tilde{\rho}_2^V$ , Eqs. (4.85) and (4.86). (b) Same for the left and right densities,  $\rho_{\text{left}}^V$  and  $\rho_{\text{right}}^V$ , Eqs. (4.88) and (4.89). The plots show the integrands including the factor  $1/(y\bar{y}^3)$  and the spin/isospin-dependent prefactors, such that they give an impression of the actual distribution of strength in the integrals.

contributes negatively to both  $\rho_1^V$  and  $\tilde{\rho}_2^V$ . The  $N$  and  $\Delta$  contributions thus tend to cancel in  $\rho_1^V$ , while they add in  $\tilde{\rho}_2^V$ . (b) The spin-dependent and -independent densities satisfy  $|\tilde{\rho}_{2,B}^V| < |\rho_{1,B}^V|$ , and the absolute values are very close  $|\tilde{\rho}_{2,B}^V| \approx |\rho_{1,B}^V|$ , for both  $B = N, \Delta$ .

Figure 6b shows the integrand of the corresponding left and right transverse densities as a function of  $y$ . The nucleon and isobar contributions obey the definiteness conditions Eqs. (4.90) and (4.91). One also observes significant differences in absolute value between the left and right densities, with  $|\rho_{\text{left},N}| \gg |\rho_{\text{right},N}|$  for the intermediate nucleon, and  $|\rho_{\text{left},\Delta}| \ll |\rho_{\text{right},\Delta}|$  for the isobar. This strong left-right asymmetry can naturally be explained in the quantum-mechanical picture in the rest frame (see Sec. V) and is a consequence of the relativistic motion of pions in chiral dynamics [8, 9].

Figures 7a and b show the densities themselves as functions of  $b$ . The densities are plotted as positive functions (note the legend) and with the exponential factor  $\exp(-2M_\pi b)$  removed, i.e., the functions shown correspond to the pre-exponential factor in Eq. (2.11). One sees that (a) the densities generated by the same intermediate state ( $B = N, \Delta$ ) have approximately the same  $b$ -dependence. (b) The isobar contribution decreases faster at large  $b$ , as is

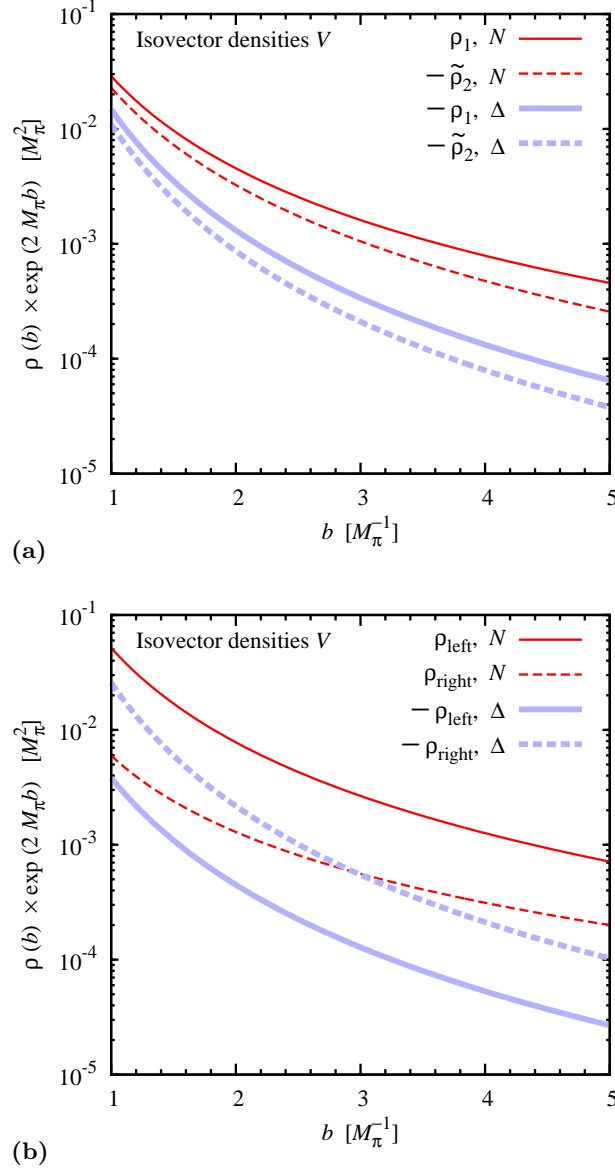


FIG. 7. Peripheral transverse densities obtained from the light-front wave function overlap integrals. The plots show the densities rescaled by  $\exp(2M_\pi b)$ , as functions of the distance  $b$ , in units of the pion mass  $M_\pi$ . (a) Intermediate  $N$  and  $\Delta$  contributions to the spin-independent and -dependent densities,  $\rho_1^V$  and  $\tilde{\rho}_2^V$ , Eqs. (4.85) and (4.86). All contributions are plotted as positive functions in order to combine them in the same graph (see the minus signs in the legend). (b) Same for the left and right densities,  $\rho_{\text{left}}^V$  and  $\rho_{\text{right}}^V$ , Eqs. (4.88) and (4.89).

expected on grounds of the larger mass of the intermediate state. (c) The left and right densities in Fig. 7b show the large left-right asymmetry observed already in the integrand.

We emphasize that the densities obtained from the light-front wave function overlap integrals, Eqs. (4.85) and (4.86), are numerically identical to those obtained by evaluating the intermediate-baryon part of the original Feynman integrals, Eq. (4.25), using the dispersive technique of Ref. [7]. This represents a crucial test of the reduction procedure of Sec. IV A and ensures the overall equivalence of the light-front representation with the invariant chiral EFT results.

## V. MECHANICAL PICTURE WITH $\Delta$ ISOBAR

### A. Transverse polarization

A particularly simple representation of the transverse charge and magnetization densities is obtained by choosing transverse spin states for the external nucleons and the intermediate baryon. The densities  $\rho_1^V$  and  $\tilde{\rho}_2^V$  are diagonal in transverse spin and permit a simple interpretation as the expectation value of the current generated by a peripheral pion in a single transverse spin state [8, 9]. We can now extend this picture to include the isobar contributions to the densities.

Transversely polarized particle states in the light-front formulation are constructed by preparing a transversely polarized state in the rest frame (we choose the  $y$ -direction) and performing the longitudinal and transverse boosts to the desired light-front momentum (cf. Sec. IV C). The bispinor for a spin-1/2 particle with transverse polarization is obtained from the general formula Eq. (4.54) by choosing the rest-frame 2-spinors as eigenspinors of the transverse spin operator  $S^y = \frac{1}{2}\sigma^y$ ,

$$\chi_{\text{tr}}(\tau = 1/2) = \frac{1}{\sqrt{2}} \begin{pmatrix} 1 \\ i \end{pmatrix}, \quad \chi_{\text{tr}}(\tau = -1/2) = \frac{1}{\sqrt{2}} \begin{pmatrix} i \\ 1 \end{pmatrix}, \quad (5.1)$$

where we use  $\tau = \pm 1/2$  to denote the  $y$ -spin eigenvalues. The polarization vector for a spin-1 particle with transverse polarization is obtained from Eqs. (4.56) and (4.57) by choosing the rest-frame 3-vectors as eigenvectors of the transverse angular momentum operator  $L^y$ , whose matrix representation is

$$(L^y)^{jk} = (-i)\epsilon^{yjk} \quad (j, k = x, y, z). \quad (5.2)$$

The eigenvectors are

$$\alpha_{\text{tr}}(\mu = \pm 1) = \frac{1}{\sqrt{2}} \begin{pmatrix} \mp 1 \\ 0 \\ i \end{pmatrix}, \quad \alpha_{\text{tr}}(\mu = 0) = \begin{pmatrix} 0 \\ 1 \\ 0 \end{pmatrix}, \quad (5.3)$$

where  $\mu = -1, 0, 1$  denotes the  $y$ -spin eigenvalues. The phase of the  $y$ -polarized spinors and vectors, Eqs. (5.1) and (5.3), is chosen such that they correspond to the result of a finite rotation of the original  $z$ -polarized spinors and vectors, Eqs. (4.55) and (4.58), by an angle of  $-\pi/2$  around the  $x$ -axis (i.e., the rotation that turns the positive  $z$ -axis into the positive  $y$ -axis, cf. Fig. 1). The vector-bispinor describing a spin-3/2 particle with transverse polarization is then given by the general formula Eq. (3.5), with the vectors and bispinors replaced by those with transverse polarization, and the summation extending over the corresponding transverse polarization labels.

With the transversely polarized spinors we can now compute the  $\pi NB$  vertex functions for transverse nucleon and baryon polarization. In the case of the intermediate nucleon ( $B = N$ ) [9] the vertex for transverse polarization is given by an expression analogous to the one for longitudinal polarization, Eq. (4.59),

$$\Gamma_{\pi NN, \text{tr}}(y, \tilde{\mathbf{k}}_T; \tau, \tau_1) = \frac{2ig_A M_N}{F_\pi \sqrt{y}} \left[ y M_N S_{\text{tr}}^z(\tau, \tau_1) + \tilde{\mathbf{k}}_T \cdot \mathbf{S}_{\text{tr}, T}(\tau, \tau_1) \right], \quad (5.4)$$

in which  $S_{\text{tr}}^z$  and  $\mathbf{S}_{\text{tr}, T} = (S_{\text{tr}}^x, S_{\text{tr}}^y)$  are the components of the 3-vector characterizing the spin transition between transversely polarized nucleon states,

$$S_{\text{tr}}^i(\tau, \tau_1) \equiv \chi_{\text{tr}}^\dagger(\tau) \left( \frac{1}{2} \sigma^i \right) \chi_{\text{tr}}(\tau_1) \quad (i = x, y, z). \quad (5.5)$$

Note that now the  $y$ -component is diagonal,

$$S_{\text{tr}}^y(\tau, \tau_1) = \tau \delta(\tau, \tau_1), \quad (5.6)$$

while the  $z$  and  $x$  components have off-diagonal terms. In the case of intermediate isobar ( $B = \Delta$ ), the vertex for transverse polarization is given by an expression analogous to the one for longitudinal polarization, Eqs. (4.61),

$$\Gamma_{\pi N \Delta, \text{tr}}(y, \tilde{\mathbf{k}}_T; \tau, \tau_1) = \sum_{\mu \tau'} C_{1, \mu; 1/2, \tau'}^{3/2, \tau} \alpha_{\text{tr}}(\mu) \cdot \mathcal{P}_{\text{tr}}(y, \tilde{\mathbf{k}}_T, \tau', \tau_1), \quad (5.7)$$

in which  $\alpha_{\text{tr}}$  is the transverse polarization 3-vector defined in Eq. (5.3), and  $\mathcal{P}_{\text{tr}} \equiv (\mathcal{P}_{\text{tr}}^z, \mathcal{P}_{\text{tr}, T})$  is given by an expression analogous to Eq. (4.62),

$$\left. \begin{array}{l} \mathcal{P}_{\text{tr}}^z \\ \mathcal{P}_{\text{tr}, T} \end{array} \right\} (y, \tilde{\mathbf{k}}_T, \tau', \tau_1) = \frac{\sqrt{2}g_{\pi N \Delta}}{M_N \tilde{y}^{3/2}} \left\{ \bar{M} \delta(\tau', \tau_1) + i \tilde{\mathbf{k}}_T \cdot [\mathbf{e}_z \times \mathbf{S}_{\text{tr}, T}(\tau', \tau_1)] \right\} \left\{ \begin{array}{l} \frac{\tilde{\mathbf{k}}_T^2}{2M_\Delta} - M_d \\ -\tilde{\mathbf{k}}_T \end{array} \right\}, \quad (5.8)$$

where now  $\mathbf{S}_{\text{tr},T}$  is the transverse  $(x, y)$  component of the 3-vector Eq. (5.5).

The  $N \rightarrow \pi B$  light-front wave function of the nucleon for transverse nucleon and baryon polarization is then given by Eq. (4.47), and its coordinate representation by Eq. (4.65), in the same way as for longitudinal polarization,

$$\Psi_{N \rightarrow \pi B, \text{tr}}(y, \tilde{\mathbf{k}}_T; \tau, \tau_1) \equiv \frac{\Gamma_{\pi NB, \text{tr}}(y, \tilde{\mathbf{k}}_T; \tau, \tau_1)}{\Delta \mathcal{M}^2(y, \tilde{\mathbf{k}}_T)}, \quad (5.9)$$

$$\Phi_{N \rightarrow \pi B, \text{tr}}(y, \mathbf{r}_T, \sigma, \sigma_1) \equiv \int \frac{d^2 \tilde{\mathbf{k}}_T}{(2\pi)^2} e^{i \tilde{\mathbf{k}}_T \cdot \mathbf{r}_T} \Psi_{N \rightarrow \pi B, \text{tr}}(y, \tilde{\mathbf{k}}_T; \sigma, \sigma_1) \quad (B = N, \Delta). \quad (5.10)$$

The general decompositions Eq. (4.70) (for the nucleon) and Eqs. (4.73)-(4.74) (for the isobar) apply to the transversely polarized coordinate-space wave function as well, as they rely only on the functional dependence of the momentum-space wave function on  $\tilde{\mathbf{k}}_T$ , not on the specific form of the spin structures. This allows us to express the transversely polarized coordinate-space wave function in terms of the radial wave functions for the longitudinally polarized system, using only the algebraic relations between the spin structures. We quote only the expressions for the components with initial transverse nucleon spin  $\tau_1 = +\frac{1}{2}$ , as they are sufficient to calculate the peripheral densities (cf. Sec. II). For the intermediate nucleon ( $B = N$ ) we obtain [9]

$$\Phi_{N \rightarrow \pi N, \text{tr}}(y, \mathbf{r}_T, \tau = +\frac{1}{2}, \tau_1 = +\frac{1}{2}) = \sin \alpha U_1, \quad (5.11)$$

$$\Phi_{N \rightarrow \pi N, \text{tr}}(y, \mathbf{r}_T, \tau = -\frac{1}{2}, \tau_1 = +\frac{1}{2}) = -U_0 + \cos \alpha U_1 \quad (5.12)$$

$$[U_{0,1} \equiv U_{0,1}(y, r_T)],$$

where  $\alpha$  denotes the angle of the transverse vector  $\mathbf{r}_T$  with respect to the  $x$ -axis,

$$\mathbf{r}_T = (r_T \cos \alpha, r_T \sin \alpha). \quad (5.13)$$

For the intermediate isobar ( $B = \Delta$ ) we obtain

$$\Phi_{N \rightarrow \pi \Delta, \text{tr}}(\mathbf{r}_T, y, \tau = +\frac{3}{2}, \tau_1 = +\frac{1}{2}) = \frac{i}{\sqrt{2}} \left[ V_0 + W_0 + (V_1 + W_1) \cos \alpha + \frac{W_2}{2} \cos 2\alpha \right], \quad (5.14)$$

$$\Phi_{N \rightarrow \pi \Delta, \text{tr}}(\mathbf{r}_T, y, \tau = +\frac{1}{2}, \tau_1 = +\frac{1}{2}) = -\frac{i}{\sqrt{6}} \left[ (V_1 + 2W_1) \sin \alpha + \frac{3W_2}{2} \sin 2\alpha \right], \quad (5.15)$$

$$\Phi_{N \rightarrow \pi \Delta, \text{tr}}(\mathbf{r}_T, y, \tau = -\frac{1}{2}, \tau_1 = +\frac{1}{2}) = \frac{i}{\sqrt{6}} \left[ V_0 + W_0 + (V_1 - W_1) \cos \alpha - \frac{3W_2}{2} \cos 2\alpha \right], \quad (5.16)$$

$$\Phi_{N \rightarrow \pi \Delta, \text{tr}}(\mathbf{r}_T, y, \tau = -\frac{3}{2}, \tau_1 = +\frac{1}{2}) = -\frac{i}{\sqrt{2}} \left[ V_1 \sin \alpha - \frac{W_2}{2} \sin 2\alpha \right] \quad (5.17)$$

$$[V_{0,1} \equiv V_{0,1}(y, r_T), W_{0,1,2} \equiv W_{0,1,2}(y, r_T)].$$

It is straightforward to compute the transverse densities in terms of the transversely polarized light-front wave functions. A simple result is obtained for the left and right current densities, Eq. (2.8):

$$\left. \begin{array}{l} \rho_{\text{left}}^V(b) \\ \rho_{\text{right}}^V(b) \end{array} \right\} = \frac{C_N}{4\pi} \int_0^1 \frac{dy}{yy^3} \left| \Phi_{N \rightarrow \pi N, \text{tr}}(y, \mp r_T \mathbf{e}_x; \tau = -\frac{1}{2}, \tau_1 = \frac{1}{2}) \right|^2, \quad (5.18)$$

$$\left. \begin{array}{l} \rho_{\text{left}}^V(b) \\ \rho_{\text{right}}^V(b) \end{array} \right\} = \frac{C_\Delta}{6\pi} \int_0^1 \frac{dy}{yy^3} \sum_{\tau = -1/2, 3/2} \left| \Phi_{N \rightarrow \pi \Delta, \text{tr}}(y, \mp r_T \mathbf{e}_x; \tau, \tau_1 = \frac{1}{2}) \right|^2 \quad (5.19)$$

$$[r_T = b/(1-y)].$$

If we substitute in Eqs. (5.18) and (5.19) the explicit expressions for  $\Phi_{N \rightarrow \pi B, \text{tr}}$  in terms of the radial wave functions, Eqs. (5.11)-(5.12) and Eqs. (5.14)-(5.14), and note that the “left” and “right” points  $\mathbf{r}_T = \mp r_T \mathbf{e}_x$  correspond to  $\alpha = \pi$  and 0, respectively [cf. Eq. (5.13)], we recover the expressions obtained previously with longitudinally polarized nucleon states, Eqs. (4.89) and (4.88). It shows that the two calculations, using transversely or longitudinally polarized nucleon states, give the same results for the densities if the  $N \rightarrow \pi B$  light-front wave functions are related as described above. We note that this correspondence is made possible by the use of light-front helicity states, which allow one to relate longitudinally and transversely polarized states in a simple manner by a rest-frame spin rotation.

The transversely polarized expressions Eqs. (5.18) and (5.19) have several remarkable properties. First, the densities are diagonal in the external nucleon transverse spin ( $\tau_2 = \tau_1$ ). They describe a sum of contributions of individual  $\pi B$  states (“orbitals”) in the nucleon’s wave function, which have definite sign and permit a simple probabilistic interpretation. Second, one sees that only specific intermediate spin states contribute to the left and right current densities on the  $x$ -axis. Parity conservation dictates that the  $\pi B$  system be in a state with odd orbital angular momentum  $L$ , such that  $(-1)^L = -1$ . Angular momentum conservation requires that the spins of the initial nucleon and the intermediate baryon and the orbital angular momentum be related by the vector coupling rule, which leaves only the state with  $L = 1$  for both  $B = N, \Delta$ . The sums in Eqs. (5.18) and (5.19) run over the intermediate baryon’s  $y$ -spin  $\tau$ , and thus effectively over the  $y$ -projection of the orbital angular momentum,

$$L^y = \tau_1 - \tau = \frac{1}{2} - \tau, \quad (5.20)$$

which can take on the values  $L^y = (-1, 0, 1)$ . Further simplification comes about because the wave function of the  $\pi B$  state with  $L^y = 0$  vanishes on the  $x$ -axis (i.e., in the direction perpendicular to the spin quantization axis), as seen in the explicit expressions Eq. (5.11) (for  $B = N$ ) and Eq. (5.15) (for  $B = \Delta$ ), which are zero for  $\alpha = 0$  or  $\pi$ . Altogether this leaves only the following intermediate states to contribute to the densities:

$N(\tau_1) \rightarrow \pi B(\tau)$			
$B$	$\tau_1$	$\tau$	$L^y$
$N$	$\frac{1}{2}$	$-\frac{1}{2}$	$1$
$\Delta$	$\frac{1}{2}$	$-\frac{1}{2}$	$1$
	$\frac{1}{2}$	$\frac{3}{2}$	$-1$

(5.21)

Thus a single orbital accounts for the transverse densities generated by the nucleon intermediate state, and two orbitals for the ones generated by the isobar. This simple structure makes the transversely polarized representation a convenient framework for studying the properties of the peripheral transverse densities in chiral EFT.

## B. Mechanical interpretation

Our results for the peripheral transverse densities with intermediate  $\Delta$  isobars can be explained in the quantum-mechanical picture described in Refs. [8, 9]. One adopts a first-quantized view of chiral EFT and follows the evolution of the chiral processes in light-front time. In this view the initial “bare” nucleon in the rest frame, with  $y$ -spin projection  $\tau_1 = +1/2$ , makes a transition to a pion-baryon (nucleon or isobar) intermediate state with baryon  $y$ -spin projection  $\tau$  and pion angular momentum projection  $L^y$  (right), and back to the bare final nucleon with  $\tau_2 = +1/2$  (see Fig. 8). The allowed quantum numbers of the intermediate states are the ones listed in Eq. (5.21). The peripheral transverse densities then arise as the result of the convection current carried by the charged pion in the intermediate state. In particular, the left and right densities,  $\rho_{\text{left}}^V(b)$  and  $\rho_{\text{right}}^V(b)$ , are given by the  $J^+$  current ( $b$ ) at the positions  $\mathbf{b} = \mp b \mathbf{e}_x$  (on the left and right  $x$ -axis, viewed from  $z = +\infty$ , cf. Fig. 1a).

In a plane-wave state the current carried by a charged pion is proportional to its 4-momentum,  $\langle \pi(k) | J^+ | \pi(k) \rangle = 2Q_\pi k^+ = 2Q_\pi [E_\pi(\mathbf{k}) + k^z]$ , where  $Q_\pi = \pm 1$  is the pion charge. The typical pion momenta in chiral EFT processes are  $|\mathbf{k}| = O(M_\pi)$ , and the energies are  $E_\pi = O(M_\pi)$ , which means that the motion of the pion is essentially relativistic. For such pions the plus current is generally much larger if  $k^z > 0$  than if  $k^z < 0$ , i.e., if the pion moves in the positive rather than the negative  $z$ -direction. Now the peripheral pion in the intermediate states of the EFT processes considered here is outside of the range of the EFT interactions (which are pointlike on the scale  $M_\pi$ ), so that its current is effectively that of a free pion (see Figure 8). One therefore concludes that the current on the side where the pion moves in the positive  $z$ -direction is much larger than on the side where it moves in the opposite direction. This basic fact explains the pattern of left and right transverse densities observed in our calculation with transversely polarized states.

In the  $\pi N$  intermediate state the only allowed transverse spin quantum numbers are  $\tau = -1/2$  and  $L^y = +1$  (see Fig. 8). In this state the pion plus current is larger on the left than on the right, so that

$$|\rho_{\text{left}, N}(b)| \gg |\rho_{\text{right}, N}(b)|. \quad (5.22)$$

This is indeed observed in the numerical results of Fig. 7b. The large left-to-right ratio of  $\sim 4 - 10$  shows that the motion of the pion is highly relativistic, because for a non-relativistic pion the left-to-right ratio would be close to

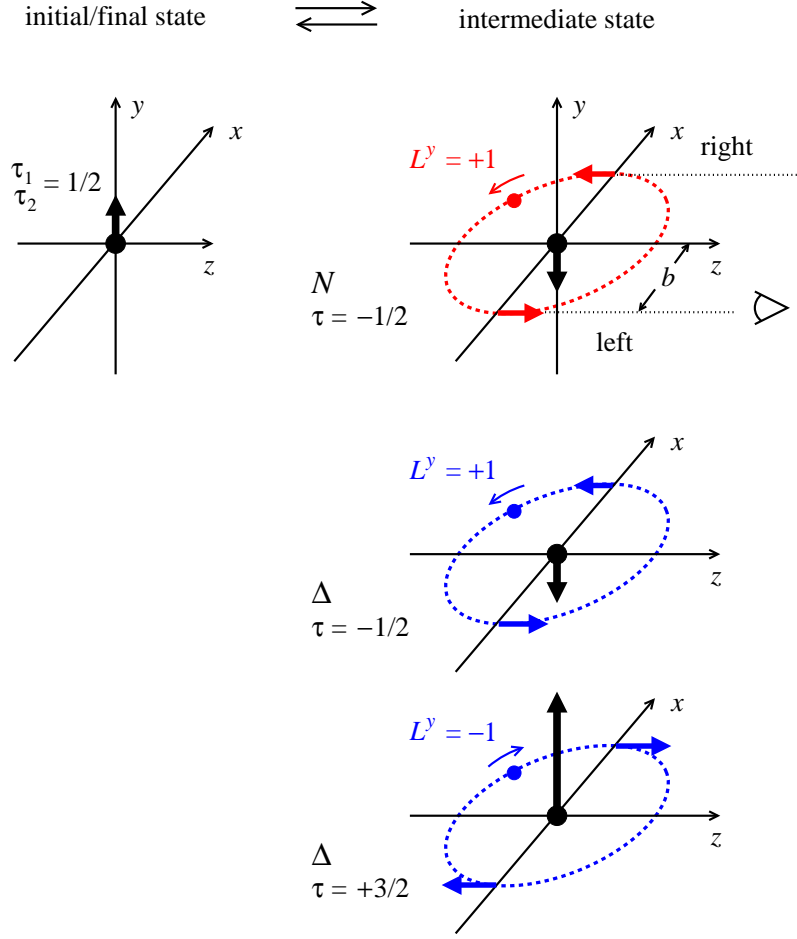


FIG. 8. Quantum-mechanical picture of the peripheral transverse densities in chiral EFT with  $\Delta$  isobars. The bare nucleon with  $y$ -spin projection  $\tau_1 = +1/2$  in the rest frame (left) makes a transition to a pion-baryon intermediate state with baryon  $y$ -spin projection  $\tau$  and pion angular momentum projection  $L^y$  (right), and back to a bare state with  $\tau_2 = +1/2$ . Top:  $\pi N$  intermediate state with  $\tau = -1/2$  and  $L^y = +1$ . Middle, bottom:  $\pi\Delta$  intermediate states with  $\tau = -1/2$  and  $L^y = +1$ , and  $\tau = +3/2$  and  $L^y = -1$ . The peripheral left/right transverse densities  $\rho_{\text{left/right}}^V(b)$  describe the  $J^+$  current at the positions  $\mathbf{b} = \mp b\mathbf{e}_x$  (on the left and right  $x$ -axis, viewed from  $z = +\infty$ ), which arises from the convection current produced by the charged pion. The spin-independent and -dependent densities,  $\rho_1^V(b)$  and  $\tilde{\rho}_2^V(b)$ , describe the left-right average and left-right asymmetry of the current (cf. Fig. 1).

unity,

$$\frac{|\rho_{\text{left},N}(b)|}{|\rho_{\text{right},N}(b)|} = 1 + O(v), \quad (5.23)$$

where  $v \ll 1$  is the characteristic velocity of the pion. In the  $\pi\Delta$  intermediate state the allowed transverse spin quantum numbers are  $\tau = -1/2$  and  $L^y = +1$ , and  $\tau = +3/2$  and  $L^y = -1$ . From the  $\pi N\Delta$  vertex for transverse polarization, Eq. (5.7), one can see that the spin wave function of the intermediate state is

$$\frac{1}{\sqrt{6}}|\tau = -\frac{1}{2}, L^y = +1\rangle + \frac{1}{\sqrt{2}}|\tau = \frac{3}{2}, L^y = -1\rangle + \dots, \quad (5.24)$$

where we omitted the components that do not contribute to the current at  $\mathbf{b} = \pm b\mathbf{e}_x$ . The configuration with  $L^y = -1$  is 3 times more likely than the one with  $L^y = 1$  and dominates the transverse densities. In the  $\pi\Delta$  intermediate states the pion therefore moves predominantly with  $L^y = -1$ , and the pion plus current is larger on the right than on the left

$$|\rho_{\text{left},\Delta}(b)| \ll |\rho_{\text{right},\Delta}(b)|. \quad (5.25)$$

This is again observed in the numerical results of Fig. 7b.

The sign of the transverse densities can be deduced by considering the isospin structure of the  $\pi B$  intermediate states. Let us consider the case that the external nucleon is a proton ( $p$ ). In  $\pi N$  intermediate states, the only configuration with a charged pion is  $\pi^+ n$ , and therefore

$$\rho_{\text{left},N}(b), \rho_{\text{right},N}(b) > 0. \quad (5.26)$$

In  $\pi\Delta$  intermediate states the isospin structure is [cf. Eq. (3.24)]

$$\frac{1}{\sqrt{2}}|\Delta^{++}\pi^-\rangle + \frac{1}{\sqrt{6}}|\Delta^0\pi^+\rangle + \frac{1}{\sqrt{3}}|\Delta^+\pi^0\rangle, \quad (5.27)$$

so that the configurations with  $\pi^-$  are 3 times more likely than the ones with  $\pi^+$ . The peripheral current is therefore dominated by the negatively charged pion, and one has

$$\rho_{\text{left},\Delta}(b), \rho_{\text{right},\Delta}(b) < 0. \quad (5.28)$$

This pattern is seen in the numerical results of Fig. 7b.

In sum, the peripheral transverse densities obtained from chiral EFT can naturally be explained in terms of the orbital motion of the peripheral pion and the isospin structure of the intermediate state in the quantum-mechanical picture. The large left-right asymmetry attests to the essentially relativistic motion of pions, which is a fundamental property of chiral dynamics [8, 9]. The  $\Delta$  isobar introduces intermediate states in which the orbital motion of the peripheral pion is “reversed” compared to the intermediate state with the nucleon, and in which the pion has “reversed” charge, resulting in a rich structure. The double reversal explains why the  $N$  and  $\Delta$  contributions compensate each other in the spin-independent density  $\rho_1^V$  but add in the spin-dependent density  $\tilde{\rho}_2^V$ . We emphasize that the mechanical picture presented here is derived from an *exact rewriting* of LO relativistic chiral EFT and has an objective dynamical content, which distinguishes it from phenomenological pion cloud models of nucleon structure.

## VI. LARGE- $N_c$ LIMIT OF TRANSVERSE DENSITIES

### A. Light-front wave functions at large $N_c$

We now want to study how the light-front representation of chiral EFT with  $\Delta$  isobars behaves in the large- $N_c$  limit of QCD. This exercise will further elucidate the structure of the wave function overlap formulas and provide a crucial test for the isobar results. It also allows us to re-derive the  $N_c$ -scaling relations for the peripheral densities in a simple manner and interpret them in the context of the mechanical picture of Sec. V.

The limit of a large number of colors in QCD represents a general method for relating properties of mesons and baryons to the microscopic theory of strong interactions [13, 14]. While even at large  $N_c$  the dynamics remains complex and cannot be solved exactly, the scaling behavior of meson and baryon properties with  $N_c$  can be established on general grounds and provides interesting insights and useful constraints for phenomenology. It is found that the masses of low-lying mesons (including the pion) scale as  $O(N_c^0)$ , while those of baryons scale as  $O(N_c)$  for states with spin/isospin  $O(N_c^0)$ . The basic hadronic size of mesons and baryons scales as  $O(N_c^0)$  and remains stable in the large- $N_c$  limit. Baryons at large  $N_c$  thus are heavy objects of fixed spatial size, whose external motion (in momentum and spin/isospin) can be described classically and is governed by inertial parameters of order  $O(N_c)$  (mass, moment of inertia). The  $N$  and  $\Delta$  appear as rotational states of the classical body with spin/isospin  $S = T = 1/2$  and  $S = T = 3/2$ , respectively, and the mass splitting is  $M_\Delta - M_N = O(N_c^{-1})$ . Further scaling relations are obtained for the transition matrix elements of current operators between meson and baryon states, as well as the meson-meson and meson-baryon couplings; see Ref. [36] for a review. The relations are model-independent and can be derived in many different ways, e.g. using diagrammatic techniques [14], group-theoretical methods [15, 16], large- $N_c$  quark models [37, 38], or the soliton picture of baryons [39, 40].

The large- $N_c$  limit can be combined with an EFT descriptions of strong interactions in terms of meson-baryon degrees of freedom, valid in special parametric regions. The application of  $N_c$ -scaling relations to chiral EFT has been studied using formal methods, focusing on the interplay of the limits  $M_\pi \rightarrow 0$  and  $N_c \rightarrow \infty$  in the calculation of spatially integrated quantities (charges, RMS radii) [12, 17, 18]. In the present study of spatial densities, following the approach of Ref. [7], we impose the  $N_c$ -scaling relations for the  $N$  and  $\Delta$  masses, and their couplings to pions, and calculate the resulting scaling behavior of the peripheral transverse densities at distances  $O(M_\pi^{-1})$ . This is consistent with our general philosophy of regarding the pion mass as finite but small on the hadronic scale,  $M_\pi \ll \mu_{\text{had}}$ , and applying chiral EFT to peripheral hadron structure at distances  $M_\pi^{-1} \gg \mu_{\text{had}}^{-1}$ .

The general  $N_c$ -scaling of the nucleon's isovector transverse charge and magnetization densities at non-exceptional distances was established in Ref. [7] and is of the form

$$\rho_1^V(b) = O(N_c^0), \quad \tilde{\rho}_2^V(b) = O(N_c) \quad [b = O(N_c^0)]. \quad (6.1)$$

These relations follow from the known  $N_c$ -scaling of the total charge and magnetic moment, and the scaling of the nucleon size as  $O(N_c^0)$ . In chiral EFT we consider the densities at peripheral distances  $b \sim M_\pi^{-1}$ . Because  $M_\pi = O(N_c^0)$ , the chiral region remains stable in the large- $N_c$  limit,

$$b \sim M_\pi^{-1} = O(N_c^0). \quad (6.2)$$

The densities generated by chiral dynamics thus represent a distinct component of the nucleon's spatial structure even in the large- $N_c$  limit. Using the dispersive representation of the transverse densities it was shown in Ref. [7] that the LO chiral EFT results obey the general  $N_c$ -scaling laws Eq. (6.1) if the isobar contribution is included.

We now want to investigate how the  $N_c$ -scaling relations for the transverse densities arise in the light-front representation of chiral EFT. To this end we consider the  $N \rightarrow \pi B$  light-front wave functions of Sec. IV with masses scaling as

$$M_N, M_\Delta = O(N_c), \quad M_\Delta - M_N = O(N_c^{-1}), \quad M_\pi = O(N_c^0). \quad (6.3)$$

The  $N_c$ -scaling of the  $\pi NN$  coupling follows from  $g_A = O(N_c)$  and  $F_\pi = O(N_c^{1/2})$  and is [cf. Eq. (3.21)]

$$g_{\pi NN} \equiv \frac{g_A M_N}{F_\pi} = O(N_c^{3/2}). \quad (6.4)$$

The  $\pi N\Delta$  coupling in the large- $N_c$  limit is related to the  $\pi NN$  coupling by [39]

$$g_{\pi N\Delta} = \frac{3}{2} g_{\pi NN} \quad (N_c \rightarrow \infty) \quad (6.5)$$

and follows the same  $N_c$ -scaling. When calculating the densities at chiral distances, Eq. (6.2), the typical pion momenta in the nucleon rest frame are  $|\mathbf{k}| \sim M_\pi = O(N_c^0)$ , and the light-front wave functions are evaluated in the region

$$\left. \begin{aligned} y &\sim M_\pi/M_N = O(N_c^{-1}) \\ |\tilde{\mathbf{k}}_T| &\sim M_\pi = O(N_c^0) \\ |\mathbf{r}_T| &\sim M_\pi^{-1} = O(N_c^0) \end{aligned} \right\}. \quad (6.6)$$

For such configurations the invariant mass denominator Eq. (4.48) is of the order

$$\Delta \mathcal{M}_{N \rightarrow \pi B}^2 = O(N_c) \quad (B = N, \Delta). \quad (6.7)$$

The  $N_c$ -scaling of the vertex function for general nucleon and baryon helicities follows from Eqs. (6.4) and (6.5),

$$\Gamma_{\pi NB} = O(N_c^{3/2}) \quad (B = N, \Delta). \quad (6.8)$$

Altogether the  $N_c$ -scaling of the light-front wave functions in the region Eq. (6.6) is

$$\left. \begin{aligned} \Psi_{N \rightarrow \pi B}(y, \tilde{\mathbf{k}}_T, \dots) &= O(N_c^{1/2}) \\ \Phi_{N \rightarrow \pi B}(y, \mathbf{r}_T, \dots) &= O(N_c^{1/2}) \end{aligned} \right\} \quad (B = N, \Delta). \quad (6.9)$$

Equation (6.9) represents the ‘‘maximal’’ scaling behavior for general nucleon and baryon helicities. Combinations of helicity components can have a lower scaling exponent due to cancellations of the leading term.

We now want to inspect the  $N_c$ -scaling of the individual helicity structures and compare the nucleon and isobar wave functions. It is straightforward to establish the scaling behavior of the radial wave functions from the explicit expressions in Eqs. (4.71) and (4.75). In the case of the intermediate nucleon ( $B = N$ ), the two radial functions are of the same order in  $N_c$ ,

$$U_0, U_1 = O(N_c^{1/2}) \quad [y = O(N_c^{-1}), r_T = O(N_c^0)]. \quad (6.10)$$

In the case of the isobar ( $B = \Delta$ ), the radial functions  $V_0$  and  $W_1$  are leading in  $N_c$ , while  $V_1, W_0$  and  $W_2$  are subleading,

$$\left. \begin{aligned} V_0, W_1 &= O(N_c^{1/2}) \\ V_1, W_0, W_2 &= O(N_c^{-1/2}) \end{aligned} \right\} [y = O(N_c^{-1}), r_T = O(N_c^0)]. \quad (6.11)$$

Furthermore, the transverse mass Eq. (4.68), which governs the radial dependence of the wave functions, becomes the same for  $B = N$  and  $\Delta$  in the large- $N_c$  limit,

$$M_{T,\Delta}^2(y) \approx M_{T,N}^2(y) \approx M_\pi^2 + y^2 M_N^2 + O(N_c^{-1}) \quad (N_c \rightarrow \infty). \quad (6.12)$$

This happens because the term proportional to the  $N$ - $\Delta$  mass splitting in Eq. (4.68) scales as  $y(M_\Delta^2 - M_N^2) = y(M_\Delta + M_N)(M_\Delta - M_N) = O(N_c^{-1})$  and is suppressed at large  $N_c$ . As a result the leading light-front wave functions for the intermediate  $N$  and  $\Delta$  at large  $N_c$  have pairwise identical radial dependence. Using also the relations between the couplings, Eq. (6.5), we obtain

$$\left. \begin{aligned} V_0(y, r_T) \\ W_1(y, r_T) \end{aligned} \right\} \approx \frac{3}{\sqrt{2}} \left\{ \begin{aligned} U_0(y, r_T) \\ U_1(y, r_T) \end{aligned} \right\} [y = O(N_c^{-1}), r_T = O(N_c^0)]. \quad (6.13)$$

The relations Eqs. (6.10)-(6.13) together embody the  $N_c$ -scaling of the full set of chiral light-front wave functions. They naturally explain the patterns observed in the intermediate  $N$  and  $\Delta$  wave functions at finite  $N_c$  (i.e., calculated with the physical baryon masses and couplings) shown in Figure 5a and b.

The  $N_c$ -scaling relations for the light-front wave functions now allow us to explain the scaling behavior of the transverse densities in a simple manner. Using Eqs. (6.10)-(6.13) in the overlap formulas, Eqs. (4.85) and (4.86), we obtain for the spin-independent density

$$\rho_{1,N}^V(b) = O(N_c), \quad \rho_{1,\Delta}^V(b) = O(N_c). \quad (6.14)$$

The scaling exponents of the intermediate  $N$  and  $\Delta$  contributions *alone* is *larger* than that of the general scaling relation Eq. (6.1). The correct  $N_c$ -scaling of the chiral EFT result is obtained by *combining* the intermediate  $N$  and  $\Delta$  contributions. Using Eq. (6.13) and the specific values of the isospin factors  $C_N$  and  $C_\Delta$ , Eq. (4.43), the  $O(N_c)$  terms cancel, and we obtain

$$\rho_{1,N}^V(b) + \rho_{1,\Delta}^V(b) = O(N_c^{-1}), \quad (6.15)$$

in accordance with Eq. (6.1). For the spin-dependent density we obtain

$$\tilde{\rho}_{2,N}^V(b) = O(N_c), \quad \tilde{\rho}_{2,\Delta}^V(b) = O(N_c), \quad (6.16)$$

Here the  $N$  and  $\Delta$  contributions alone already show the correct scaling behavior as required by Eq. (6.1). Using Eqs. (6.13) and (4.43) one sees that in the large- $N_c$  limit the intermediate  $\Delta$  contribution is exactly 1/2 times the intermediate  $N$  one, so that the combined result is 3/2 times the  $N$  contribution alone,

$$\tilde{\rho}_{2,\Delta}^V(b) = \frac{1}{2} \tilde{\rho}_{2,N}^V(b) + O(N_c^{-1}), \quad (6.17)$$

$$\tilde{\rho}_{2,N}^V(b) + \tilde{\rho}_{2,\Delta}^V(b) = \frac{3}{2} \tilde{\rho}_{2,N}^V(b) + O(N_c^{-1}), \quad (6.18)$$

as found in the dispersive calculation of Ref. [7]. Altogether, we see that the chiral EFT results with the isobar reproduce the general  $N_c$ -scaling of the transverse densities. In the mechanical picture of Sec. V, Eq. (6.15) is realized by the cancellation of the currents produced by the peripheral pion in states with intermediate  $N$  and  $\Delta$ ; Eq.(6.18), by the addition of the same currents.

## B. Contact terms and off-shell behavior

We now want to evaluate the contact term contributions to the peripheral transverse densities and verify that they, too, obey the general  $N_c$ -scaling laws. This exercise also exposes the effect of the off-shell ambiguity of the chiral EFT with isobars on the peripheral densities, and shows to what extent the ambiguity can be constrained by  $N_c$ -scaling arguments.

Following the decomposition of the LO current matrix element in Sec. IV A, the peripheral densities are given by the sum of the intermediate-baryon and contact terms,<sup>4</sup>

$$\left. \begin{aligned} \rho_{1,B}^V(b) &= \rho_{1,B}^V(b)_{\text{interm}} + \rho_{1,B}^V(b)_{\text{cont}} \\ \tilde{\rho}_{2,B}^V(b) &= \tilde{\rho}_{2,B}^V(b)_{\text{interm}} + \tilde{\rho}_{2,B}^V(b)_{\text{cont}} \end{aligned} \right\} \quad (B = N, \Delta). \quad (6.19)$$

The intermediate-baryon terms were expressed as light-front wave function overlap in Sec. IV B, and their  $N_c$ -scaling studied in Sec. VI A. The contact terms are computed by evaluating the Feynman integrals, Eqs. (4.5) and (4.7), and Eqs. (4.20) and (4.22), directly as four-dimensional integrals, using the fact that they depend on the 4-momentum transfer  $\Delta$  as the only external 4-vector [7]. We obtain

$$\rho_{1,N}^V(b)_{\text{cont}} = \frac{(1 - g_A^2)M_\pi^4}{12\pi^3 F_\pi^2} R_{\text{cont}}(M_\pi b), \quad (6.20)$$

$$\rho_{1,\Delta}^V(b)_{\text{cont}} = \frac{g_{\pi N\Delta}^2 M_\pi^4 (M_\Delta + M_N)^2}{108\pi^3 M_\Delta^2 M_N^2} R_{\text{cont}}(M_\pi b), \quad (6.21)$$

$$\tilde{\rho}_{2,N}^V(b)_{\text{cont}} = 0, \quad (6.22)$$

$$\tilde{\rho}_{2,\Delta}^V(b)_{\text{cont}} = \frac{g_{\pi N\Delta}^2 M_\pi^5}{108\pi^3 M_\Delta^2 M_N} R'_{\text{cont}}(M_\pi b), \quad (6.23)$$

where  $R_{\text{cont}}$  denotes the normalized loop integral introduced in Appendix B of Ref. [7] ( $\beta = M_\pi b$ )

$$R_{\text{cont}}(\beta) \equiv \frac{1}{16} \{3[K_0(\beta)]^2 - 4[K_1(\beta)]^2 + [K_2(\beta)]^2\}, \quad (6.24)$$

$$R'_{\text{cont}}(\beta) \equiv \frac{\partial}{\partial\beta} R_{\text{cont}}(\beta) = \frac{1}{16} [-2K_0(\beta)K_1(\beta) + 3K_1(\beta)K_2(\beta) - K_2(\beta)K_3(\beta)]. \quad (6.25)$$

In deriving Eq. (6.21) we have neglected terms  $O(M_\pi^2/M_N^2)$  in the coefficient; this approximation is consistent with both the chiral and the  $1/N_c$  expansions, and the neglected terms are numerically small.

We can now study the  $N_c$ -scaling of the contact terms. In the spin-independent density  $\rho_1^V$  we observe that

$$\rho_{1,N}^V(b)_{\text{cont}} = O(N_c), \quad (6.26)$$

$$\rho_{1,\Delta}^V(b)_{\text{cont}} = O(N_c), \quad (6.27)$$

$$\rho_{1,\Delta}^V(b)_{\text{cont}} + \rho_{1,N}^V(b)_{\text{cont}} = O(N_c^0). \quad (6.28)$$

The  $N$  and  $\Delta$  contact terms are individually  $O(N_c)$ , as the intermediate-baryon terms, but they cancel each other in leading order, as it should be. This remarkable result comes about thanks to two circumstances: (a) in the  $N$  contact term the piece proportional to  $g_A^2 = O(N_c^2)$  dominates; this piece arises from the nucleon triangle diagram and has the same origin as the  $\Delta$  contact term; (b) the coupling constants in the large- $N_c$  limit are related by Eqs. (6.4) and (6.5). Note that the contact and intermediate-baryon terms are of the same order in  $N_c$  in the spin-independent density,

$$\frac{\rho_{1,B}^V(b)_{\text{cont}}}{\rho_{1,B}^V(b)_{\text{interm}}} = O(N_c^0) \quad (B = N, \Delta). \quad (6.29)$$

The cancellation between the nucleon and isobar contact terms, Eq. (6.28), is thus essential in bringing about the correct  $N_c$ -scaling of the overall spin-independent densities. In the spin-dependent density  $\tilde{\rho}_2^V$  there is no contribution from the nucleon contact term in LO of the chiral expansion (a non-zero contribution appears at NLO and scales as  $O(N_c^{-1})$  and is therefore suppressed in large- $N_c$  limit [7, 31]). The isobar contact term Eq. (6.23) scales as

$$\tilde{\rho}_{2,\Delta}^V(b)_{\text{cont}} = O(N_c^{-1}), \quad (6.30)$$

---

<sup>4</sup> In this section we use explicit labels “interm” and “cont” to denote the intermediate-baryon and contact contribution to the densities; cf. Footnote 3.

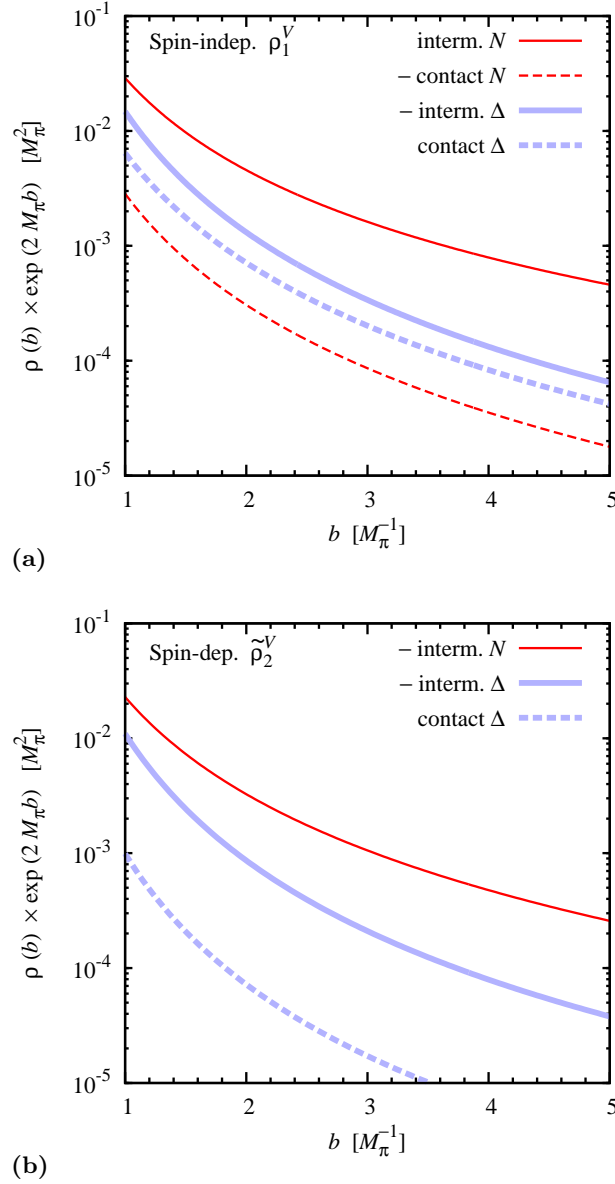


FIG. 9. Intermediate-baryon and contact term contributions to the peripheral transverse densities.

and is therefore of the same order in  $N_c$  as the nucleon contact term, as is natural. Both nucleon and isobar contact terms are therefore strongly suppressed relative to the intermediate-baryon terms in the spin-dependent density,

$$\frac{\tilde{\rho}_{2,B}^V(b)_{\text{cont}}}{\tilde{\rho}_{2,B}^V(b)_{\text{interm}}} = O(N_c^{-2}) \quad (B = N, \Delta). \quad (6.31)$$

In sum, the full peripheral densities, including the contact terms, obey the same large- $N_c$  relations as the intermediate-baryon contributions represented by the light-front wave function overlap integrals. In the spin-independent case this comes about due to a non-trivial cancellation between the nucleon and isobar contact terms.

Numerical results for the contact term densities are shown in Fig. 9a and b. Their dependence on the distance  $b$  is similar to that of the intermediate-baryon contributions in the region of interest. The magnitude and sign of the densities follow the pattern implied by the large- $N_c$  limit.

The findings regarding the  $N_c$ -scaling of the contact terms have implications for the off-shell behavior of the EFT including isobars (cf. Sec. III). In the present calculation we take into account only contact terms resulting from the off-shell behavior of the  $\Delta$  propagator and vertices, but do not include any explicit “new”  $\pi\pi NN$  contact terms associated with the introduction of the  $\Delta$ . Our results show that this prescription gives the correct  $N_c$ -scaling of the

transverse densities. From the perspective of the large- $N_c$  limit there is thus *no need* to introduce explicit contact terms. This is positive, as it allows us to perform a consistent calculation with the minimal off-shell extension. It is also negative, as it means that  $N_c$ -scaling alone is not sufficient to fix the off-shell ambiguity of chiral EFT with isobars. Answers to this question have to come from dynamical considerations beyond the large- $N_c$  limit [41]. In this sense the numerical results for the contact term densities should be regarded as estimates, as they may be modified by  $1/N_c$ -suppressed off-shell terms, which we cannot determine within the present scheme.

An advantage of the light-front representation of chiral EFT with isobars is that the effects of the off-shell ambiguity are entirely contained in the contact term contributions to the densities. The wave function overlap contribution (as defined in the scheme of Sec. IV A) relies only on the on-shell properties of the EFT. As such this representation is very efficient and might be of more general use in studying the off-shell ambiguities of chiral EFT with high-spin particles.

## VII. SUMMARY AND OUTLOOK

In this work we have included the  $\Delta$  isobar in the light-front representation of chiral EFT and studied its effect on the nucleon's peripheral transverse densities. We have done this by systematically rewriting of the relativistically invariant chiral EFT results in a form that they correspond to  $N \rightarrow \pi B$  ( $B = N, \Delta$ ) light-front wave function overlap and contact terms. The resulting expressions give rise to a simple quantum-mechanical picture, expose the role of pion orbital angular momentum in chiral processes, and illustrate the essentially relativistic nature of chiral dynamics. They also permit a concise derivation of the  $N_c$ -scaling relations and numerical evaluation of the peripheral densities. It is worth emphasizing that (a) the light-front representation presented here is *exactly equivalent* to the relativistically invariant chiral EFT results, which implies that rotational invariance is effectively preserved in our approach; (b) the quantum-mechanical picture described here is based on chiral EFT interactions and has an objective physical meaning, which distinguishes it from phenomenological pion cloud models or other models of transverse nucleon structure.

The  $\Delta$  isobar affects the transverse densities both parametrically and numerically. Parametrically it restores the proper scaling behavior of the peripheral densities in the large- $N_c$  limit. The scaling behavior involves both the light-front wave function overlap and the contact terms, and provides a non-trivial test of the formalism. Numerically we find that the intermediate isobar contributions are of moderate size in the spin-dependent and -independent densities,  $\rho_1(b)$  and  $\tilde{\rho}_2(b)$ , amounting to  $\sim 30\%$ – $10\%$  of the intermediate nucleon contributions at  $b = 1\text{--}5 M_\pi^{-1}$ . The isobar contributions become very substantial in the right current density  $\rho_{\text{right}} = \rho_1 + \tilde{\rho}_2$ , in which the nucleon contribution is small, and inclusion of the isobar reverses the sign of the density at  $b \lesssim 3 M_\pi^{-1}$ .

The practical issues in extracting peripheral transverse densities from elastic form factor data and testing the chiral predictions have been discussed in Refs. [6–8]. Because the analytic properties of the form factors (especially the two-pion cut at  $t > 4M_\pi^2$ ) are critically important in the Fourier transform at large distances, one must use dispersive fits to the form factor data when extracting the peripheral densities. A dispersive analysis of the transverse densities has shown that the chiral component becomes dominant at  $b \gtrsim 2 \text{ fm} \sim 1.4 M_\pi^{-1}$ ; at smaller distances the densities are dominated by the  $\rho$  meson resonance [42]. A detailed phenomenological study of the uncertainties of the peripheral densities, using dispersive fits to present form factor data and including their theoretical uncertainties, should be undertaken in the future.

The theoretical methods developed in this study could be applied to several other problems of interest. The derivation of the light-front representation from invariant integrals in Secs. IV A and IV B represents a general scheme that could be applied to EFTs with other high-spin particles, or to matrix elements of higher-spin operators such as those describing moments of generalized parton distributions (twist-2, spin- $n$  operators,  $n \geq 1$ ). It should generally be useful in situations where rotational invariance is critical (e.g., to avoid power-like divergences) and a relativistically invariant formulation is available. One obvious example are the nucleon form factors of the energy-momentum tensor (twist-2, spin-2 operator), which describe the distribution of momentum, mass, and forces in the nucleon and are an object of intense study in connection with nucleon spin problem; see Ref. [43] for a review.

In the present study we calculate the transverse densities in the nucleon and consider the isobar as an intermediate state in the peripheral chiral processes. The same formalism would allow one to calculate also the transverse densities associated with the  $N \rightarrow \Delta$  transition form factors, for which chiral EFT results and experimental data are available [44–46]. The peripheral current matrix element between the spin-1/2 and spin-3/2 states contain structures with orbital angular momentum  $\Delta L = 0, 1$  and  $2$ , which could be illustrated in the mechanical picture of Sec. V. The formalism could be applied just as well to the transverse densities in the isobar state itself, associated with the  $\Delta \rightarrow \Delta$  form factors, which are a well-defined concept in the context of chiral EFT [47, 48], and are studied also in Lattice QCD [49–51].

## ACKNOWLEDGMENTS

We thank J. M. Alarcon and J. Goity for helpful discussions of questions regarding chiral EFT and the  $\Delta$  isobar.

This material is based upon work supported by the U.S. Department of Energy, Office of Science, Office of Nuclear Physics under contract DE-AC05-06OR23177.

- 
- [1] D. E. Soper, Phys. Rev. D **15**, 1141 (1977).  
[2] M. Burkardt, Phys. Rev. D **62**, 071503 (2000) [Erratum-ibid. D **66**, 119903 (2002)] [hep-ph/0005108].  
[3] M. Burkardt, Int. J. Mod. Phys. A **18**, 173 (2003) [hep-ph/0207047].  
[4] G. A. Miller, Phys. Rev. Lett. **99**, 112001 (2007) [arXiv:0705.2409 [nucl-th]].  
[5] G. A. Miller, Ann. Rev. Nucl. Part. Sci. **60**, 1 (2010) [arXiv:1002.0355 [nucl-th]].  
[6] M. Strikman and C. Weiss, Phys. Rev. C **82**, 042201 (2010) [arXiv:1004.3535 [hep-ph]].  
[7] C. Granados and C. Weiss, JHEP **1401**, 092 (2014) [arXiv:1308.1634 [hep-ph]].  
[8] C. Granados and C. Weiss, JHEP **1507**, 170 (2015) [arXiv:1503.04839 [hep-ph]].  
[9] C. Granados and C. Weiss, Phys. Rev. C **92**, 025206 (2015) [arXiv:1503.02055 [hep-ph]].  
[10] T. R. Hemmert, B. R. Holstein and J. Kambor, J. Phys. G **24** (1998) 1831 [hep-ph/9712496].  
[11] V. Pascalutsa, M. Vanderhaeghen and S. N. Yang, Phys. Rept. **437**, 125 (2007) [hep-ph/0609004].  
[12] A. C. Cordon and J. L. Goity, Phys. Rev. D **87**, 016019 (2013) [arXiv:1210.2364 [nucl-th]].  
[13] G. 't Hooft, Nucl. Phys. B **72**, 461 (1974).  
[14] E. Witten, Nucl. Phys. B **160**, 57 (1979).  
[15] R. F. Dashen, E. E. Jenkins and A. V. Manohar, Phys. Rev. D **49**, 4713 (1994) [Erratum-ibid. D **51**, 2489 (1995)] [hep-ph/9310379].  
[16] R. F. Dashen, E. E. Jenkins and A. V. Manohar, Phys. Rev. D **51**, 3697 (1995) [hep-ph/9411234].  
[17] T. D. Cohen and W. Broniowski, Phys. Lett. B **292**, 5 (1992) [hep-ph/9208253].  
[18] T. D. Cohen, Rev. Mod. Phys. **68**, 599 (1996).  
[19] M. Strikman and C. Weiss, Phys. Rev. D **69**, 054012 (2004) [hep-ph/0308191].  
[20] M. Strikman and C. Weiss, Phys. Rev. D **80**, 114029 (2009) [arXiv:0906.3267 [hep-ph]].  
[21] C. R. Ji, W. Melnitchouk and A. W. Thomas, Phys. Rev. D **80**, 054018 (2009) [arXiv:0906.3497 [nucl-th]].  
[22] M. Burkardt, K. S. Hendricks, C. R. Ji, W. Melnitchouk and A. W. Thomas, Phys. Rev. D **87**, 056009 (2013) [arXiv:1211.5853 [hep-ph]].  
[23] C. R. Ji, W. Melnitchouk and A. W. Thomas, Phys. Rev. D **88**, 076005 (2013) [arXiv:1306.6073 [hep-ph]].  
[24] V. Pascalutsa and R. Timmermans, Phys. Rev. C **60**, 042201 (1999) [nucl-th/9905065].  
[25] V. Pascalutsa, Phys. Lett. B **503**, 85 (2001) [hep-ph/0008026].  
[26] P. A. M. Dirac, Rev. Mod. Phys. **21**, 392 (1949).  
[27] H. Leutwyler and J. Stern, Annals Phys. **112**, 94 (1978).  
[28] S. J. Brodsky, H. -C. Pauli and S. S. Pinsky, Phys. Rept. **301**, 299 (1998) [hep-ph/9705477].  
[29] J. Gasser, M. E. Sainio and A. Svarc, Nucl. Phys. B **307**, 779 (1988).  
[30] V. Bernard, N. Kaiser, J. Kambor and U.-G. Meissner, Nucl. Phys. B **388**, 315 (1992).  
[31] B. Kubis and U.-G. Meissner, Nucl. Phys. A **679**, 698 (2001) [hep-ph/0007056].  
[32] N. Kaiser, Phys. Rev. C **68**, 025202 (2003) [nucl-th/0302072].  
[33] T. Becher and H. Leutwyler, Eur. Phys. J. C **9**, 643 (1999) [hep-ph/9901384].  
[34] V. B. Berestetskii, E. M. Lifshitz and L. P. Pitaevskii, in: Course of Theoretical Physics, Vol. IV: Relativistic Quantum Theory, Pergamon Press, Oxford, 1973.  
[35] Z. Dziembowski, H. Holtmann, A. Szczurek and J. Speth, Annals Phys. **258**, 1 (1997).  
[36] E. E. Jenkins, Ann. Rev. Nucl. Part. Sci. **48**, 81 (1998) [hep-ph/9803349].  
[37] G. Karl and J. E. Paton, Phys. Rev. D **30**, 238 (1984).  
[38] A. Jackson, A. D. Jackson and V. Pasquier, Nucl. Phys. A **432**, 567 (1985).  
[39] G. S. Adkins, C. R. Nappi and E. Witten, Nucl. Phys. B **228**, 552 (1983).  
[40] I. Zahed and G. E. Brown, Phys. Rept. **142**, 1 (1986).  
[41] J. M. Alarcon *et al.*, in preparation.  
[42] G. A. Miller, M. Strikman and C. Weiss, Phys. Rev. C **84**, 045205 (2011) [arXiv:1105.6364 [hep-ph]].  
[43] E. Leader and C. Lorce, Phys. Rept. **541**, 163 (2014) [arXiv:1309.4235 [hep-ph]].  
[44] V. Pascalutsa and M. Vanderhaeghen, Phys. Rev. Lett. **95**, 232001 (2005) [hep-ph/0508060].  
[45] V. Pascalutsa and M. Vanderhaeghen, Phys. Rev. D **76**, 111501 (2007) [arXiv:0711.0147 [hep-ph]].  
[46] C. E. Carlson and M. Vanderhaeghen, Phys. Rev. Lett. **100**, 032004 (2008) [arXiv:0710.0835 [hep-ph]].  
[47] T. Ledwig, V. Pascalutsa and M. Vanderhaeghen, Phys. Rev. D **82**, 091301 (2010) [arXiv:1004.5055 [hep-ph]].  
[48] T. Ledwig, J. Martin-Camalich, V. Pascalutsa and M. Vanderhaeghen, Phys. Rev. D **85**, 034013 (2012) [arXiv:1108.2523 [hep-ph]].  
[49] C. Alexandrou, T. Korzec, G. Koutsou, C. Lorce, J. W. Negele, V. Pascalutsa, A. Tsapalis and M. Vanderhaeghen, Nucl. Phys. A **825**, 115 (2009) [arXiv:0901.3457 [hep-ph]].

[50] C. Alexandrou *et al.*, Phys. Rev. D **79**, 014507 (2009) [arXiv:0810.3976 [hep-lat]].

[51] C. Aubin, K. Orginos, V. Pascalutsa and M. Vanderhaeghen, Phys. Rev. D **79**, 051502 (2009) [arXiv:0811.2440 [hep-lat]].